

**In search of a castle:
Multisensor UAS research at the
Medieval site of 't Huijs ten Bosch, Weesp**

Jitte Waagen



UNIVERSITY OF AMSTERDAM



4D Research Lab

The 4D Research Lab Report Series has been established as an instrument to promote transparency regarding the 4DRL virtual visualisation projects, workflow and pipeline development and technical experiments. The aim is to maximize knowledge sharing, meta- and paradata communication and clarification of author- and ownership of 4D Research Lab products.

The 4DRL Report Series is published under a CC-BY license.

Jitte Waagen, Tijm Lanjouw

In search of a castle:
Multisensor UAS research at the
Medieval site of 't Huijs ten Bosch, Weesp

4D Research Lab Report Series 4

Author(s): Jitte Waagen
Layout: Mikko Kriek
Editor(s): Jitte Waagen, Tijm Lanjouw

ISSN 2772-7734

June 2023

<http://4dresearchlab.nl>

1 Project datasheet

Name project	Multisensor UAS research at the Medieval site of Huis ten Bosch, Weesp
Date (from – to)	01/2022 – 09/2022
Author of report	Jitte Waagen, 4D Research Lab
Project initiators	Ranjith Jayasena, Gemeente Amsterdam, Monumenten en Archeologie
Execution	Jitte Waagen, 4D Research Lab: project management, fieldwork, research, data modeling, reporting Tijm Lanjouw, 4D Research Lab: fieldwork Mikko Kriek, 4D Research Lab: fieldwork Markus Stoffer, 4D Research Lab: fieldwork
Scientific advice	NA
Delivered product(s)	Projected sensor data, raster files, generated maps/visualisations
Where to access main outcomes/product	Available on request at the 4D Research Lab. Contact Jitte Waagen (j.waagen@uva.nl).
Location and accessibility of project files	4D Research Lab archive, cloud storage. Available on request at the 4D Research Lab. Contact Jitte Waagen (j.waagen@uva.nl)
Related publications	NA

2 Aims and justification

2.1 *Abstract*

The drone remote sensing operations were initially commissioned by Monumenten en Archeologie of the Gemeente Amsterdam, by archaeologist Dr. Ranjith Jayasena. The site under investigation is the Medieval castle 't Huijs ten Bosch, built after 1220 and destroyed in 1672, still visible as earthworks and cropmarks as a rectangular structure. The project entails an investigation into both the application and comparative value of innovative sensor techniques for prospection purposes as well as nature, extent, and state of preservation of the site itself (KNA Protocol 4003 Inventariserend Veldonderzoek 4.1: verkennend, karterend, waarderend veldonderzoek).

2.2 *Introduction*

2.2.1 *Overview: site and research questions*

The specific aim of the drone remote sensing operations has been twofold; first, they have been part of a comparative study into innovative prospection techniques in the Dutch landscape, and second, they are part of a broader investigation into the nature, extent, and preservation of the Medieval site.

The site at Huis ten Bosch is a castle of Medieval origin, situated at Gooilandsdijk 7, in an open field used as grassland (fig. 1). Based on historical sources, the castle was erected in the 13th century AD, after which it is supposed to have been besieged, destroyed, and rebuilt several times, until it was finally razed by a French army in 1672. As property of the feudal family of Amstel, it plays an important role in the early development of the Medieval city of Amsterdam and related power plays (Jayasena 2023). The site itself however has never been archaeologically researched, and little is known about the typology and extent of the fortification(s), nor about the nature and state of eventual preserved subsoil archaeological remains. There are some earthworks (e.g., fig. 4) and cropmarks indicating a square tower structure and an abutting wall, oriented east-west, as well as some vegetation marks that indicate additional disturbances of the subsoil. However, they do not provide a solid basis for answering the above questions.

The comparative study into the value of drone remote sensing techniques is important for several reasons. The flexibility of drone operations renders their deployment for archaeological prospection purposes a very interesting avenue of innovation (Waagen et al. 2022, Rensink et al. 2022). For example, their ability to take-off and fly anywhere (within legal regulations), the relative speed of data collection, combined with the high-resolution sensor data resulting from it, as well as the reduction of atmospheric attenuation because of the close distance to the earth surface are very beneficial for archaeological purposes. However, there are still many unknowns as to the effectiveness of various sensors in different types of landscapes. Important questions to answer for example are: in what season and for what vegetation are multispectral recordings effective; which variables related to soil typology, atmospheric conditions and material properties affect the potential for thermal infrared recordings to pick up buried archaeology; what is the added value of the in-



Figure 1. Research area, left: location of 't Huijs ten Bosch near Weesp, right: main research area.

creased resolution of UAS-based LiDAR recording in comparison with the Algemeen Hoogtebestand Nederland (AHN). Finding answers to these questions is of pivotal importance for future effective implementation of these techniques in research designs and the KNA, and therefore need careful comparative research. This involves deployment of these various sensors on different types of sites in different types of soils, flying in different seasons with different atmospheric conditions, and experimenting with different technical workflows. Very important as well is the possibility to validate the mapped anomalies in order to be able to understand their relative potential. Therefore, this research is a case study that is part of a larger investigation into the potential of drone remote sensing and is a very important case because of the different methods of prospection archaeology deployed.

In the course of 2022, three fieldwork operations have been executed, making use of optical, thermal infrared, multispectral and LiDAR sensors. Their basic workings are described here, with their potential output for archaeological prospection, as well as main point of interest from a methodological point of view.

2.2.2 Optical

Optical sensors, i.e., visible-light cameras, can be deployed using UAS platforms to collect high-resolution aerial photographs. Using photogrammetric techniques through a combination of computer vision and geometrical triangulation, individual photos can be relatively positioned, and their pixel data combined to project 3D points, create a 3D mesh and project photorealistic textures on that mesh. The mesh as well as 3D point clouds can be used to create, among other products, both mosaicked aerial orthophotos and Digital Elevation Models, that can help identify crop-marks and soil marks, as well as earthworks. Furthermore, they are very valuable for comparison with other sensor data to understand whether identified anomalies are likely archaeological features, or may be explained by other human-, topographical or landscape features.

Methodological questions: optical sensors, and drone platforms to mount them under, can be relatively cheap, so the potential of deriving both high-quality aerial

imagery as well as elevation data that can match or even result in better data than LiDAR-derived Digital Elevation Models, is very interesting. In addition, data can be collected at any time, optimizing the possibility to detect crop- and soil marks. However, fieldwork is more involved as you need for example ground control and favourable atmospheric conditions. Photogrammetric postprocessing is also a rather complex process vulnerable to many variables determining the eventual output. Research therein involves comparing the workflows and outputs with data derived from other sources such as national geographic data portals (AHN, satellite imagery, etc.).

2.2.3 *LiDAR (Light Detection and Ranging)*

Aerial laser scanning is deployed to collect a dense point cloud consisting of 3D coordinates of the earth's surface. LiDAR scanners often incorporate optical cameras to attribute colours to the individual points, so products of LiDAR can be both high-resolution Digital Elevation Models and 3D coloured meshes. A specific advantage of LiDAR technology is the possibility of producing so-called Ground-Point models; a part of the laser pulses will reach the earth surface regardless of the vegetations, which means it is possible to map micromorphology, including earthworks, that remain otherwise invisible under the canopy.

Methodological questions: LiDAR sensors, and drone platforms to mount them under, are relatively expensive, but the workflow is relatively straightforward, and fieldwork is less involved than using aerial photogrammetry. LiDAR data is freely available as the AHN for the Netherlands, in a resolution of 1 point every 20 cm. The main question therefore is what the added value of drone-mounted LiDAR sensors here may be. In relation to the AHN, drone-mounted LiDAR can easily measure 1 point in a single square cm, and even in higher resolutions, however, does this result in any significant increase in archaeological information that can be extracted? Also, as drone-mounted LiDAR can be deployed in any time of the year, i.e., in any vegetation condition, it can avoid noise caused by low vegetation; but again, is there a significant increase in archaeological information that can then be extracted? Research therein involves comparing the outputs with data derived from other sources such as UAS photogrammetry and the national AHN dataset.

2.2.4 *Multispectral*

Multispectral sensors record visible light as well as part of the invisible electromagnetic spectrum in separate bands on different sensors, resulting in different reflectance images, typically Blue (centre wavelength: 475 nm), Green (centre wavelength: 560 nm), Red (centre wavelength: 668 nm), Rededge (centre wavelength: 772 nm), and Near-Infrared (centre wavelength: 840 nm), although different combinations and (slightly diverging) wavelengths are possible. Since the degree to which different materials absorb or reflect radiation of different wavelengths, the exact reflectance values can provide information about their physical compositions. This can make observations possible beyond human eyesight; for example, cropmarks can be

greatly enhanced because more healthy vegetation reflects relatively more Near-Infrared radiation but absorbs more visible light. Using photogrammetric techniques similar as with optical data, mosaicked reflectance maps can be created. The various wavelength reflectance maps can be part of many equations that emphasize various aspects of vegetation, for example Normalized Difference Vegetation Index (NDVI) often used for agricultural purposes.

Methodological questions: multispectral sensors, and drone platforms to mount them under, can be relatively affordable, so the potential of deriving high-quality multispectral imagery is very interesting. Compared to satellite multispectral images, resolution is significantly increased, and atmospheric attenuation decreased. Similar with optical sensors, data can be collected at any time, optimizing the possibility to detect crop- and soil marks. However, fieldwork is more involved as you need for example ground control and favourable atmospheric conditions, and photogrammetric postprocessing is a rather complex process vulnerable to many variables determining the eventual output. In addition, the potential of multispectral imaging to detect archaeological features is dependent on vegetation types and growth cycles, and the field of derivative analysis is rapidly evolving. Research therefore involves comparing the workflows and outputs with data derived from other sources such as optical sensors, but also study of soil- and vegetation types and annual cycles, in combination with repeating multispectral recording at different moments in the year.

2.2.5 *Thermal Imaging*

Thermal sensors record thermal infrared radiation typically in the range between 8 and 14 μm in the electromagnetic spectrum. Materials emit the thermal infrared radiation absorbed in sunlight, with emission values depending on their thermodynamic properties. In specific circumstances (Waagen et al. 2022), archaeological features can be detected in thermograms. Such features may appear as anomalies caused by different physical compositions of materials and soil, for example because they have a larger volumetric heat capacity, meaning that they can absorb more heat and thus stay warm longer after sunset. For example, ditches dug and backfilled in the past may have higher moisture content that cools down slower during the course of the night, and thus result in a thermal anomaly. Such spectral or thermal marks can therefore point to surface features as well as to buried deposits. Using photogrammetric techniques similar as with optical data, mosaicked reflectance maps can be created.

Methodological questions: drone thermography opened up a new toolset for archaeological prospection, as it results in much more useful datasets than thermal imagery from satellites that is much more affected by atmospheric attenuation. However, thermal infrared sensors, and drone platforms to mount them under, range a lot in costs, and there are many variables affecting the potential of archaeological features to be registered as spectral marks. Therefore, the research into drone thermography is still in an experimental phase, where effective sensors and platforms are being tested, as well as the full breadth of variables possibly affecting their efficacy; atmospheric conditions, diurnal and longer-term temperature flux,

season, covering- and matrix soil types, material types and their respective thermodynamic properties, etc. Research thereinto involves comparing the workflows and outputs in many different contexts, landscapes, sites and recording moments, as well as study of soil- and vegetation types, in combination with repeating thermal recording at different moments in the year.

3 Historical context

The castle is expected to be of a motte and bailey type, as was common in the 13th century, probably built in brick. As there have been some destruction and rebuilding phases, it can be expected that the terrain has seen various phases of building activity, at the one hand probably extending the buildings, and at the other also creating palimpsest effects with regard to the older building phases.

The castle has been visualised in several drawings, such as that from the collection Atlas Schoenmaker, but all have been made after its final destruction (fig. 2). Therefore, it is uncertain whether the structures that are depicted on these sources, and that may indicate a bailey and other associated buildings, have actually been present. The most likely parallel may be castle Nederhemert, which is a direct geographical and chronological parallel to Huis ten Bosch and shows an apparently similar layout with a square fortified tower in a corner, of a small courtyard surrounded by castle walls (fig. 3).

For further historical context, please see Jayasena (2023).



Figure 2. 't Huijs ten Bosch near Weesp, *Atlas Schoemaker*, 1710-1735. Source: Noord-Hollands Archief.

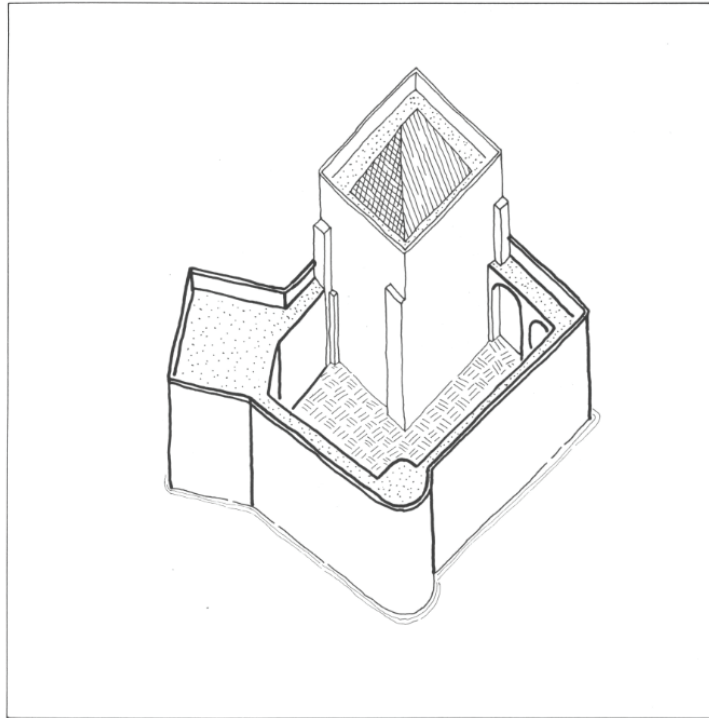


Figure 3. Castle Nederhemert, phase 2, ca. 1325 AD.

4 Documentation and research design

The original campaign in February 2022 was commissioned by the Municipality of Amsterdam; however, because of the comparative research possibilities, two more drone operations, one in June and one in September were organised by the 4D Research Lab.

4.1 *Reality based documentation and modelling workflows.*

This section elaborates on the data acquisition procedure per sensor and documentation workflow adapted from Lozić and Štular (2021) with modifications for different sensor types.

4.1.1 *Raw data acquisition and processing*

Visits to the site have been in February 2022, in June 2022 and in September 2022. The flight operations in February were part of a larger plan with visits of local people, media (NH-nieuws, AT5) and aldermen of the Municipality of Amsterdam. The flight conditions were not optimal; the ground was very wet due to intermittent rain, 75% relative humidity, most of the time a dense cloud cover and the temperature 9 degrees Celsius on average, with very small changes between day and night (8 min – 11 max). Flight moments were set for optimal results, i.e., optical at noon (solar angle at maximum zenith), multispectral within 2 hours of the solar noon and thermal after sunset. However, due to the drizzle starting after 5 minutes of flight, the thermal recording was aborted. The flight altitudes were set to result in an optimal Ground Sample Distance (GSD), around 1 cm/pixel for the optical recordings, and around 3 cm/pixel for the multispectral recording.

The flight operations in June (fig. 4 and 5) were scheduled under a bit of time pressure, resulting in a multispectral and thermal recording, but the optical recording abandoned. This decision was acceptable, as it is possible to produce an RGB index based on the separate band recordings of the multispectral camera. The flight conditions were fine, with dry weather and a clear sky, 72% relative humidity, and the temperature 13 degrees Celsius on average, with very considerable changes between day and night (4 min – 19 max). Flight moments were set for optimal results, i.e., multispectral within 2 hours of the solar noon and thermal after sunset. The flight altitudes were set to result in an optimal GSD, around 3 cm/pixel for the multispectral recording and 23 cm/pixel for the thermal infrared recording.

Finally, the flight operations in September have been the most extensive. Due to a long period of drought, vegetation stress resulted in a lot of cropmarks. Unfortunately, due to fieldwork abroad, the flight operation moment was relatively late in the month, and grass had already been cut. Whereas this did not eradicate the cropmarks, the tractor activity left a lot of tracks intersecting the cropmarks and here and there obscuring sharp observation. The flight conditions were again fine, with dry weather and few scattered clouds, 75% relative humidity, and the temperature 16 degrees Celsius on average, with very slight changes between day and night (13 min – 18 max). Flight moments were set for optimal results, i.e., optical at noon (solar



Figure 4. Research area, photo taken in June 2022 from the north towards the south, with the accentuation in the terrain clearly visible to the right.



Figure 5. Materials, photos taken in June 2022, left: DJI M210 (l) and DJI M300 (r), right: DJI M210 aloft.

angle at maximum zenith), multispectral within 2 hours of the solar noon and thermal after sunset. The flight altitudes were set to result in an optimal GSD but a bit higher than earlier capturing moments so a bit more of the surrounding area could be covered. This resulted in around 1.5 cm/pixel for the optical recording, around 7 cm/pixel for the multispectral recording and 16.5 cm/pixel for the thermal infrared recording. We were also able to collect LiDAR data during these operations, as a test for its usefulness on sites such as this. In a very short flight of around 5 minutes, 122 million points were collected with a very high density per sqm, eventually aimed at a GSD of 1 point per sqcm. Due to the flight strip adjustment not yet perfectly calibrated, the data collected shows some striping. See appendix 1 for the documented data capture parameters.

4.1.2 Data Processing and Derivation of the Products

Data processing is shortly described here per type of data, as the procedures are different for each datatype.

Optical sensor data

For the optical datasets, processing is rather straightforward. Geotagged images are, after a quick manual inspection on quality, imported into photogrammetric software, in this case Pix4D. They are integrated with the differential GPS data in form of geolocated targets that are visible on the images. Images are run through a process of internal and external alignment (called calibration in Pix4D), dense point cloud and 3D mesh generation and finally processed into digital elevation models and orthophotos (for technical explanations, see e.g., Sapirstein and Murray 2017). Final visualisation is done by generating a multiband colour (RGB) raster that can be directly imported and inspected in GIS (QGIS).

Multispectral sensor data

For the multispectral datasets, processing is a bit more involved. Five different images are generated in every single capture moment (using [...]_1.tif, [...]_2.tif etc. suffixes): one individual image for every specific bandwidth storing the captured reflectance values in respectively the Red (R), Green (G), Blue (B), Rededge (RE) and Near Infrared (NIR) band. Again, geotagged images are, after a quick manual inspection on quality, imported into photogrammetric software, in this case Pix4D. Here, they are calibrated using the photos made in the field of the reflectance target as well as the data in the EXIF of the Downwelling Light Sensor. This compensates for any major changes in the radiation from the sun during the recording and between recordings. Then, using the set of images with the reflectance in the Green band, the process follows the common photogrammetric procedure; images are integrated with the differential GPS data in the form of geolocated targets that are visible on the images; images are run through a process of internal and external alignment (called calibration in Pix4D), and a dense point cloud is generated.

Based on the generated point cloud index maps can be generated. The captured reflectance in the different bands is projected onto the individual pixels of a generated orthophoto, which are the RGB, RE and NIR bands. The different reflectance

values can also be used to generate different kinds of indices, usually called Vegetation Indices (VIs). The software allows to make such calculations and generate new index maps. A very common example is the Normalized Difference Vegetation Index (NDVI) indicating relative plant health, calculated by:

$$NDVI = \frac{(NIR - R)}{(NIR + R)}$$

Among other indices generated, the NDVI turned out to be the most informative, and has been included in this report. Eventual visualisation is done by importing and inspecting the different indices in GIS (QGIS). Raster values can be visualised using the singleband pseudocolour option. For this project, the interactive local cumulative cut stretch toolset of QGIS has been used to generate different enhanced visualisations.

Thermal infrared sensor data

The thermal images are first calibrated using thermal imaging software (FLIR Thermal Studio Pro), where distance to the subject, relative humidity and such factors are used to adjust recorded radiation values. The resulting thermograms are of the radiometric type, which means they have the actual recorded values as metadata attached as a 14-bit dataset, instead of a relative distribution of 256 grayscale values representing the range of recorded radiation (Waagen et al. 2022). These images have the suffix [..]_R.JPG. After manual inspection, thermograms are imported into photogrammetric software (Pix4D), and then the process follows the common photogrammetric procedure; images are integrated with the differential GPS data in form of geolocated targets that are visible on the images; images are run through a process of internal and external alignment (called calibration in Pix4D), and a dense point cloud is generated.

Based on the generated point cloud a reflectance map can be generated. Similar to the multispectral raster derivatives, eventual visualisation is done by importing and inspecting the reflectance map in GIS (QGIS) and raster values can be visualised using the singleband pseudocolour option. For various reasons, thermograms can feature a global temperature change in one direction (i.e., from thermal drift, see Hill et al. 2020). Therefore, the raster datasets have been corrected using the following procedure: generate a 30m low pass filter to extract the global trend in reflectance values, project that onto a new raster and subtract this global trend raster from the original reflectance map. In this way, local contrasts in reflectance values can be much better analysed. Additionally, for this project, the interactive local cumulative cut stretch toolset of QGIS has been used to generate different enhanced visualisations.

LiDAR sensor data

The LiDAR data produced by the DJI Zenmuse L1 scanner is of a proprietary DJI format .LDR and needs to be processed in DJI Terra (free version) to generate a registered (geolocated) point cloud of all recorded points. Exported JPG images that are produced by the integrated optical camera are used in this process to attribute a colour intensity value to the individual points. It can then be exported in a .LAS format for further postprocessing. The free version of Rapidlasso GmbH LASStools was then

used to subsequently tile the points (to allow for efficient batch-processing), classify the points, extract the ground points (as opposed to trees, buildings, infrastructure, etc.) and interpolate those into individual digital terrain models (DTMs). During the tiling, which has been set at 10x10 m tiles, the points have been decimated to maximum 10k points per tile, to arrive at a 1 cm resolution. More would have been redundant, as well as would have caused a lot of additional processing time. Finally, because of ease of use, GIS (QGIS) was then used to merge those into a single DTM. Eventual visualisation is done by importing and inspecting the DTM in GIS (QGIS). Raster values can be visualised using the singleband pseudocolour option. For this project, the interactive local cumulative cut stretch toolset of QGIS has been used to generate different enhanced visualisations.

See appendix 2 for the documented data processing parameters.

4.1.3 (Archaeological) interpretation

The archaeological interpretation is a stepped process. First of all, visualisation leads to first identification of potential anomalies, and comparative analysis provides clues as to their origins. Anomalies are mostly identified through relative contrasts in sensor readings. Although the sensors do provide accurate elevation points, temperatures, reflectance values, etc., such absolute values are largely not directly relevant for archaeological prospection purposes. The interpretation process starts with an integrative approach in which all contextual data is retrieved (e.g., from online data portals) and added to the dataset. Anomalies will be compared with all other data layers in order to be able to isolate the potential archaeological evidence. In a subsequent step, identified anomalies, i.e., a data model based on relative sensor readings of features that cannot be clearly explained by natural or modern anthropomorphic activity, will be evaluated in terms of potential archaeological interpretation. This process is mostly guided through contextual and typological analyses, and eventually results in an archaeological model. It must be mentioned that this often plays out as an iterative process between primary data processing, enhanced visualisation, and mapping interpretation.

Contextual data

Contextual data for this project was available as satellite imagery from both Google Earth and the *satellietdataportal.nl*. Also, various data layers available through *Publieke Dienstverlening op de Kaart* (PDOK plugin in QGIS) have been inspected, i.e., 25cm aerial photographs and thermal infrared coverage. Also, the AHN3 has been downloaded and inspected (<https://www.pdok.nl/downloads/-/article/actueel-hoogtebestand-nederland-ahn3>). Since the study of these datasets have already been reported on in a preceding inventory, they will not be elaborately dealt with here.

In general, the satellite images (fig. 6) show what is also clear during field assessment. Rectangular crop marks in the northwest part of the field close to the modern farm, such as on the 2021 image, indicate the presence of square tower walls and abutting castle walls. On the 2007 image, earthworks can be discerned as cast shad-



Figure 6. Satellite imagery, left from 2007, right from 2021.



Figure 7. AHN3 data, 0.5 m digital terrain model, here visualized fused with a hillshade model.

ow in the field, again indicating the presence of the abutting castle walls as well as some other contours that are difficult to interpret.

The AHN3 data (fig. 7), filtered on ground points, shows already quite a bit more detail. The aforementioned tower and castle walls are clearly visible here as minute elevation differences, as well as some possible abutting walls to the south of the square tower. In the rest of the field, linear and rectangular features can be discerned, which are again subtle differences in terrain height.

Mapping and interpretation

Following the workflows described above, a total of 55 anomalies have been identified. They are discussed in detail in this section. Anomalies have been mapped on the layers in which they appear the clearest, they have not been marked on every single visualised data model to avoid redundancy. Some anomalies that are clearly different on various layers have been marked multiple times. Please note that not all data layers from all flights have been included in the discussion of the results, but only those that provided clear anomalies.

See appendix 3 for a description of the documented metadata in the table.

February 2022, orthophoto (optical sensor)



Figures 8-11. Optical mosaics from February 2022, without and with annotated anomalies.



All mapping (fig. 8-11) by JW, 29-03-2023 (all vegetation densities: 1)

id	source_lay	anoma_int	an_confid	visibility	arch_int	arch_confi
18	opt_ortho_rgb	muddy area/low grass density	3	2	digging in the past	1
19	opt_ortho_rgb	moist area	3	2	none	0
20	opt_ortho_rgb	moist area	3	2	none	0
21	opt_ortho_rgb	moist area	3	2	none	0
22	opt_ortho_rgb	muddy area/low grass density	3	2	none	0
23	opt_ortho_rgb	muddy area/low grass density	3	2	depression due to moat	2
24	opt_ortho_rgb	cropmark, different vegetation	3	2	recent digging, stone removal	1
25	opt_ortho_rgb	cropmark, different vegetation	3	2	recent digging, stone removal	1
26	opt_ortho_rgb	cropmark, different vegetation	3	2	recent digging, stone removal	1
27	opt_ortho_rgb	cropmark, different vegetation	3	2	recent digging, stone removal	1
28	opt_ortho_rgb	cropmark, different vegetation	3	2	recent digging, stone removal	1
29	opt_ortho_rgb	cropmark, different vegetation	3	2	recent digging, stone removal	1
30	opt_ortho_rgb	cropmark, different vegetation	3	2	recent digging, stone removal	1
31	opt_ortho_rgb	cropmark, different vegetation	3	2	recent digging, stone removal	1
45	opt_ortho_rgb	cropmark, different vegetation	3	2	recent digging, stone removal	1
46	opt_ortho_rgb	moist area	3	2	none	0

Remarks

The cropmarks 24-29 and 45 are all brownish vegetation patches (there are more dispersed through the mapped area, not all have been marked), that in the June recordings features low bushes. They are close or exactly overlap the expected castle walls trajectory. These may be traces of digging activities for stone removal.

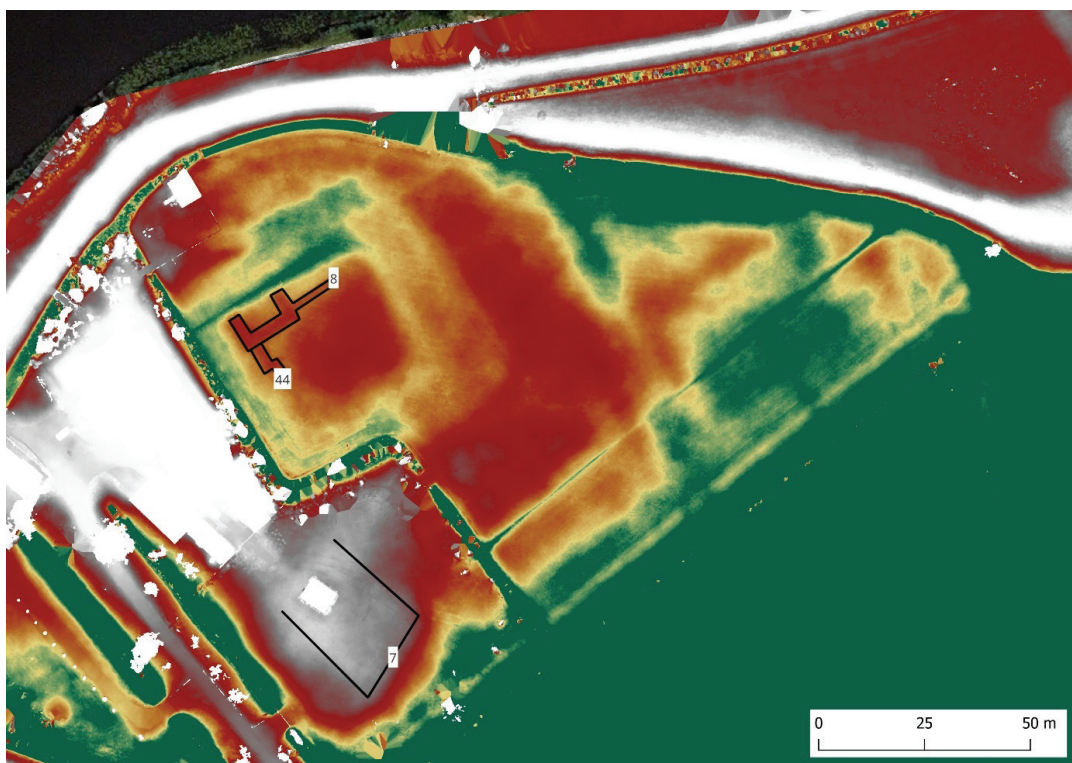
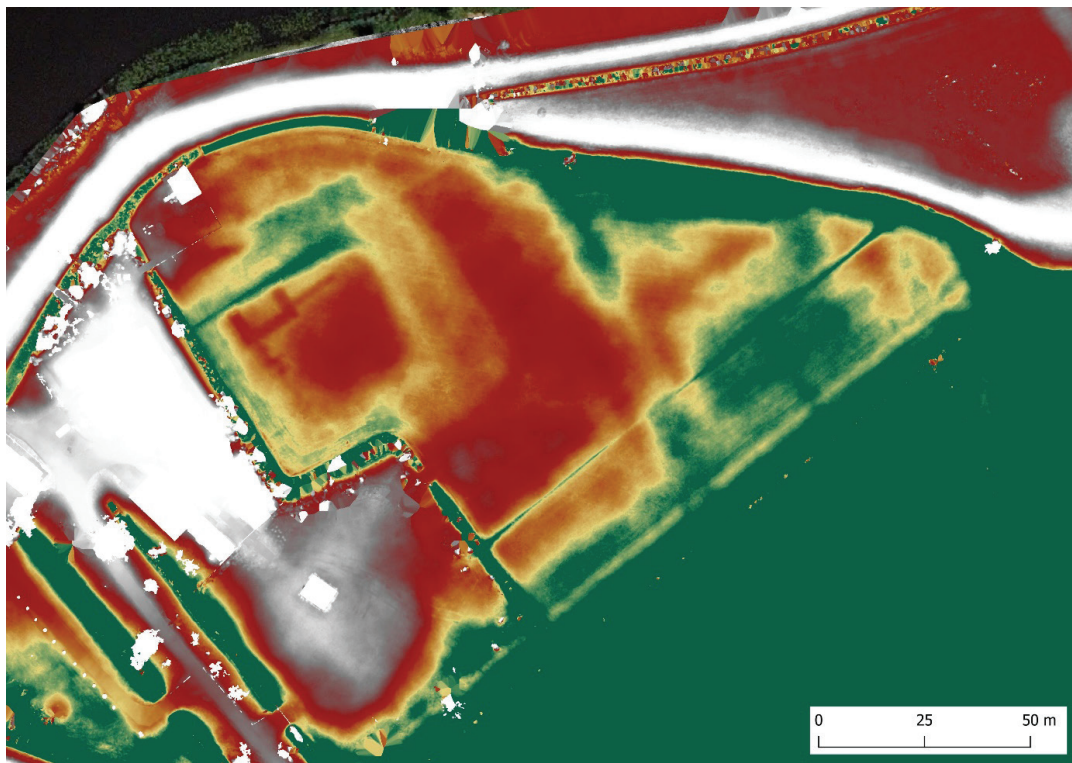
The similar cropmarks 30-31 may confirm the above hypothesis; they are located exactly on the location where a continuation of the tower walls is expected (which are clear on many different data layers); a watering gully appears to have been dug here, and the stones that should have been here are not visible on any of the data layers. They likely have been removed.

Cropmark 18 then is an elongated brownish/less dense patch of vegetation that exactly follows the tower and castle walls. There may be a more porous soil matrix affecting vegetation growth here. Can this point to digging activities, or maybe an old excavation?

Moist/muddy patch of land anomaly 23 then is located in a slightly depressed part that must have been part of the original moat, which is why water flows off here towards the modern ditch.

Moist/muddy patches 19-22 all lie in the lower parts of the field, which is unremarkable, but have been marked as anomalies because they overlap (19-21, 46) or lie parallel to (22) other identified anomalies and may be related.

February 2022, DSM (optical sensor)



Figures 12-13. DSM from February 2022, without and with annotated anomalies.

All mapping (fig. 12-13) by JW, 29-03-2023 (all vegetation densities: 1)

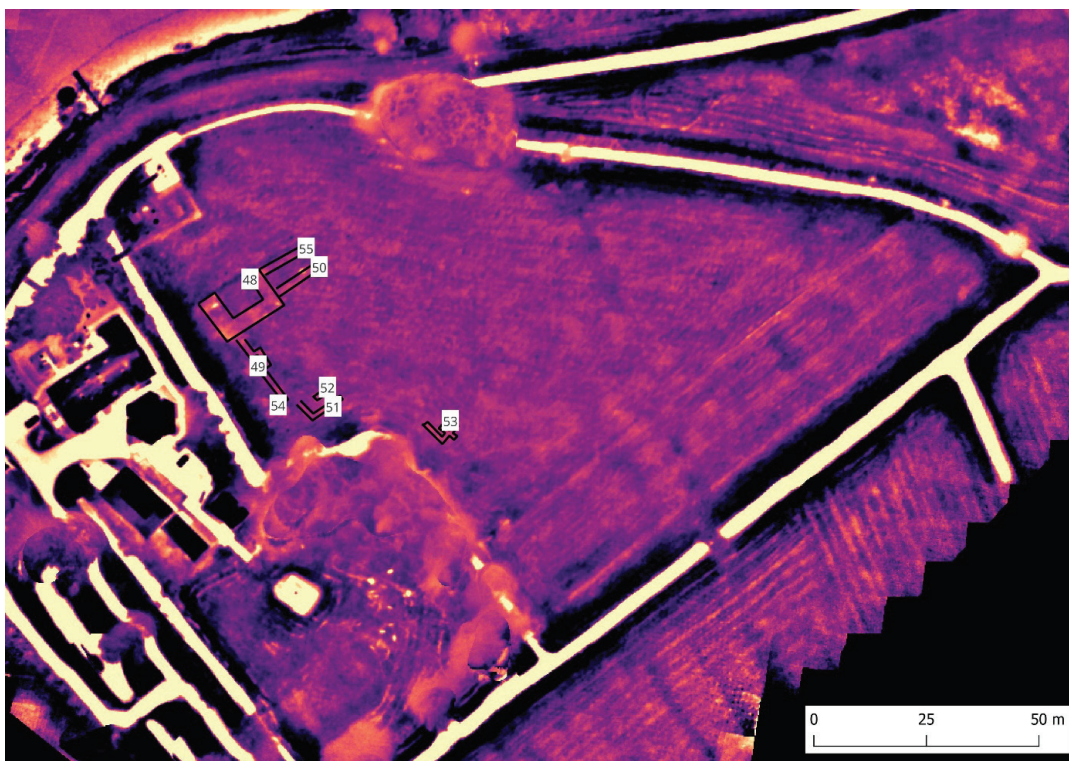
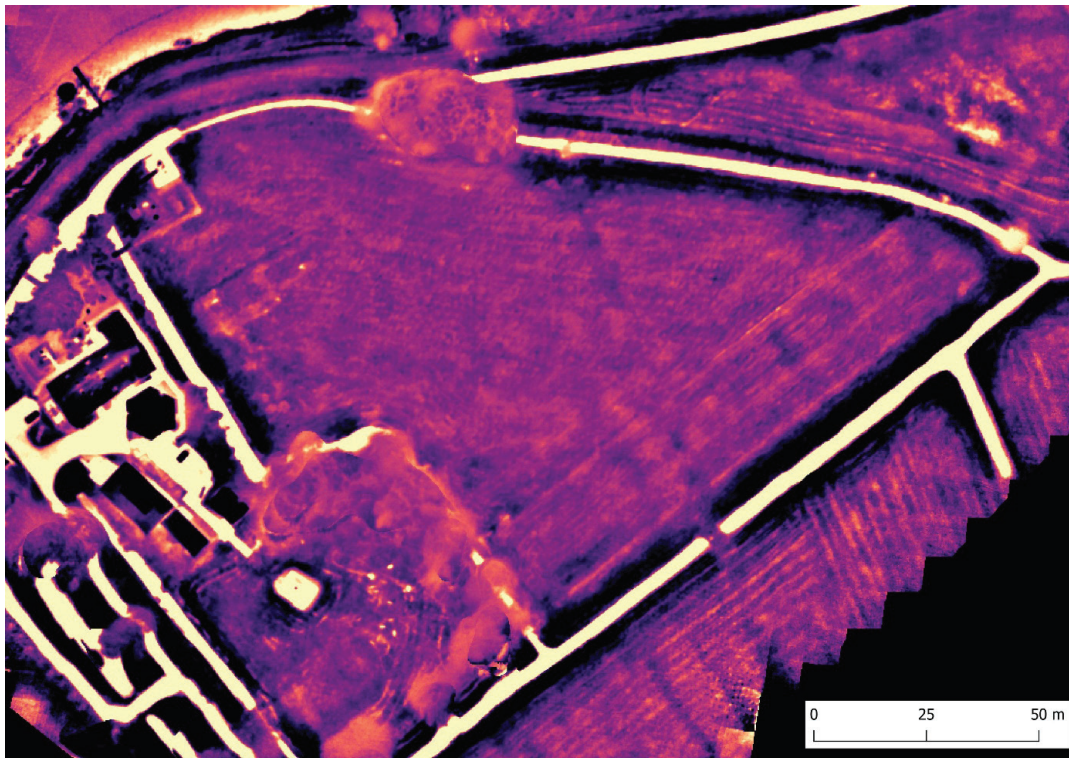
id	source_lay	anoma_int	an_confid	visibility	arch_int	arch_conf
7	opt_dsm_loc_hist_str	rectangular-ish elevated area	0	1	none	0
8	opt_dsm_loc_hist_str	elevated rectangular features	3	2	stone tower/ castle walls	3
44	opt_dsm_loc_hist_str	elevated rectangular features	3	2	stone castle walls	3

Remarks

Anomaly 7 has been marked because of its rectangular-ish shape that does not at first glance appear as a result from the similar oriented subrecent structure on the terrain, although on the optical orthophoto it appears as if there has been ploughing in these directions.

Earthworks 8 and 44 are very clear; these are elevated rectangular features, of which 8 can also be clearly seen in the field and on all recordings, and 44 on some other recordings. Feature 8 can be interpreted as tower and castle walls, and feature 44 as walls forming a structure abutting the inside of the western castle wall.

June 2022, thermal mosaic (thermal sensor)



Figures 14-15. Thermal mosaic from June 2022, without and with annotated anomalies.

All mapping (fig. 14-15) by JW, 11-05-2023 (all vegetation densities: 1)

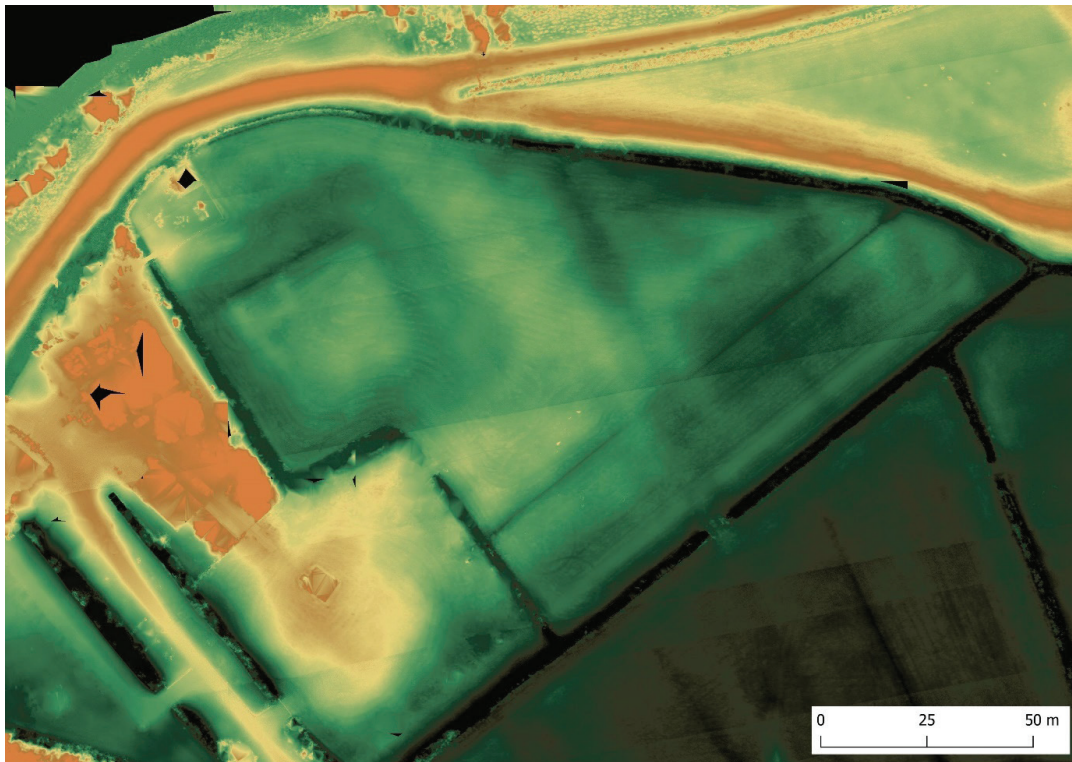
id	source_lay	anoma_int	an_confid	visibility	arch_int	arch_confid
48	therm_100m_ LP_30m	spectral mark, rectangular fea- ture	3	2	stone tower/castle walls	3
49	therm_100m_ LP_30m	spectral mark, rectangular fea- ture	3	2	stone castle struc- tures	3
50	therm_100m_ LP_30m	spectral mark, rectangular fea- ture	3	2	stone castle struc- tures	3
51	therm_100m_ LP_30m	spectral mark, rectangular fea- ture	3	2	stone castle struc- tures	3
52	therm_100m_ LP_30m	spectral mark, rectangular fea- ture	3	2	stone castle struc- tures	3
53	therm_100m_ LP_30m	spectral mark, rectangular fea- ture	2	2	stone walls	2
54	therm_100m_ LP_30m	spectral mark, rectangular fea- ture	3	2	stone castle struc- tures	3
55	therm_100m_ LP_30m	spectral mark, rectangular fea- ture	3	2	stone castle struc- tures	3

Remarks

All spectral marks identified as anomalies are lighter on the thermal mosaic, meaning that they emit more thermal radiation than the direct surrounding soil matrix. Features 48, 50 and 55 are clearly anomalies indicating the tower and castle walls, visible because of buried stones that retain a relatively high amount of heat. Anomalies 49, 51, 52 and 54 are slightly less clear but still due to their shape and orientation likely signal stone walls.

Anomaly 53 is similar in clarity as the probable stone walls of 49, 51, 52 and 54 and could also point to buried stone walls, though is rather isolated and not clearly interpretable as a specific type of structure.

September 2022, DTM (LiDAR sensor)



Figures 16-17. LiDAR generated DTM from September 2022, without and with annotated anomalies.

All mapping (fig. 16-17) by JW, 29-03-2023 (all vegetation densities: 1)

id	source_lay	anoma_int	an_confid	visibility	arch_int	arch_confi
1	dem_1cmres	ditch outline	3	2	moat outline	3
2	dem_1cmres	rectangular elevation	1	1	stone debris of collapsed wall	1
3	dem_1cmres	outline of rectangular depression	1	2	field/structure boundary	1
4	dem_1cmres	ditch outline	3	2	secondary moat outline	1
5	dem_1cmres	ditch outline	1	1	none	0
6	dem_1cmres	edge of slightly elevated area	1	1	field/structure boundary	1

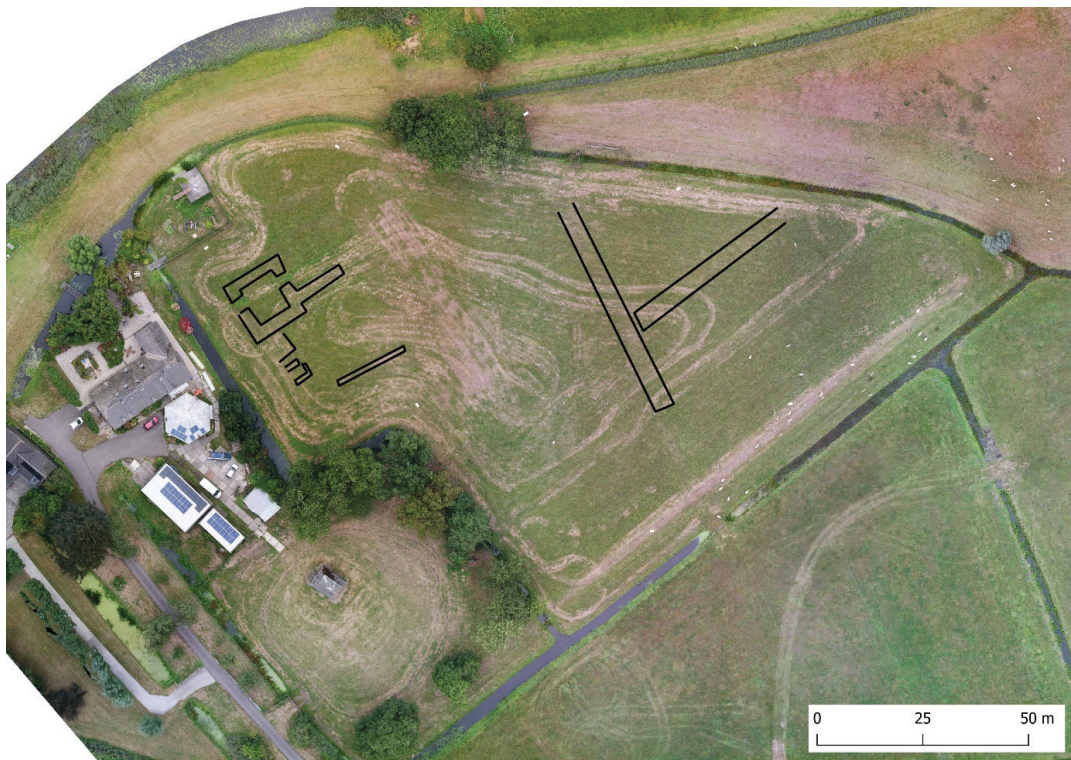
Remarks

Anomaly 1 can quite clearly be interpreted as the outline of the moat surrounding the motte; its width is on average 15m. Anomaly 2 then is a slightly elevated straight ridge of terrain in the moat, that appears to be present in the northern and eastern part of the moat depression. It may signal remains of building materials in the moat, such as parts of a collapsed castle wall, although the line is quite neat and one could expect a more diffuse pattern of fallen building material.

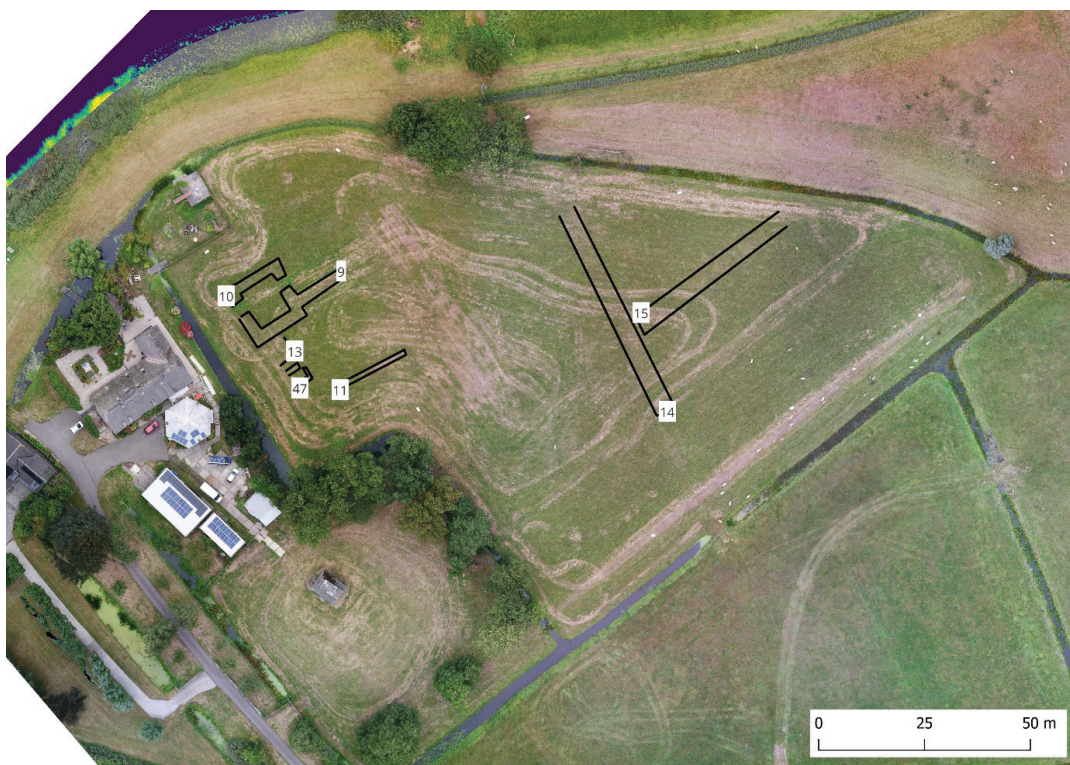
Anomalies 4 and 5 are slight depressions in the field, that follow straight/angular trajectories, and may be indicative of old ditches, or maybe even a secondary moat (4)?

Anomalies 5 and 6 are slightly elevated edges/ridges in the field that appear to run parallel to the orientation of the castle walls and the moat. It is not clear what these may point to, but maybe they are remnants of the layout of fields or structures in relation to the motte.

September 2022, orthophoto (optical sensor)



Figures 18-20. Optical mosaics from September 2022, without, with anomalies and with annotated anomalies.



All mapping (fig. 18-20) by JW, 29-03-2023 (all vegetation densities: 1)

id	source_lay	anoma_int	an_confid	visibility	arch_int	arch_confi
9	opt_ortho_rgb	cropmark, rec- tangular dry area	3	2	stone tower/castle walls	3
10	opt_ortho_rgb	cropmark, rec- tangular dry area	3	2	stone tower walls	3
11	opt_ortho_rgb	cropmark, rec- tangular dry area	2	2	stone castle struc- tures	2
12	opt_ortho_rgb	cropmark, rec- tangular dry area	2	2	stone castle struc- tures	2
13	opt_ortho_rgb	cropmark, rec- tangular dry area	2	2	stone castle struc- tures	2
14	opt_ortho_rgb	cropmark, rec- tangular dry area	3	2	secondary moat outline	1
15	opt_ortho_rgb	cropmark, rec- tangular dry area	3	2	ditch	1
47	opt_ortho_rgb	cropmark, rec- tangular dry area	2	2	stone castle struc- tures	2

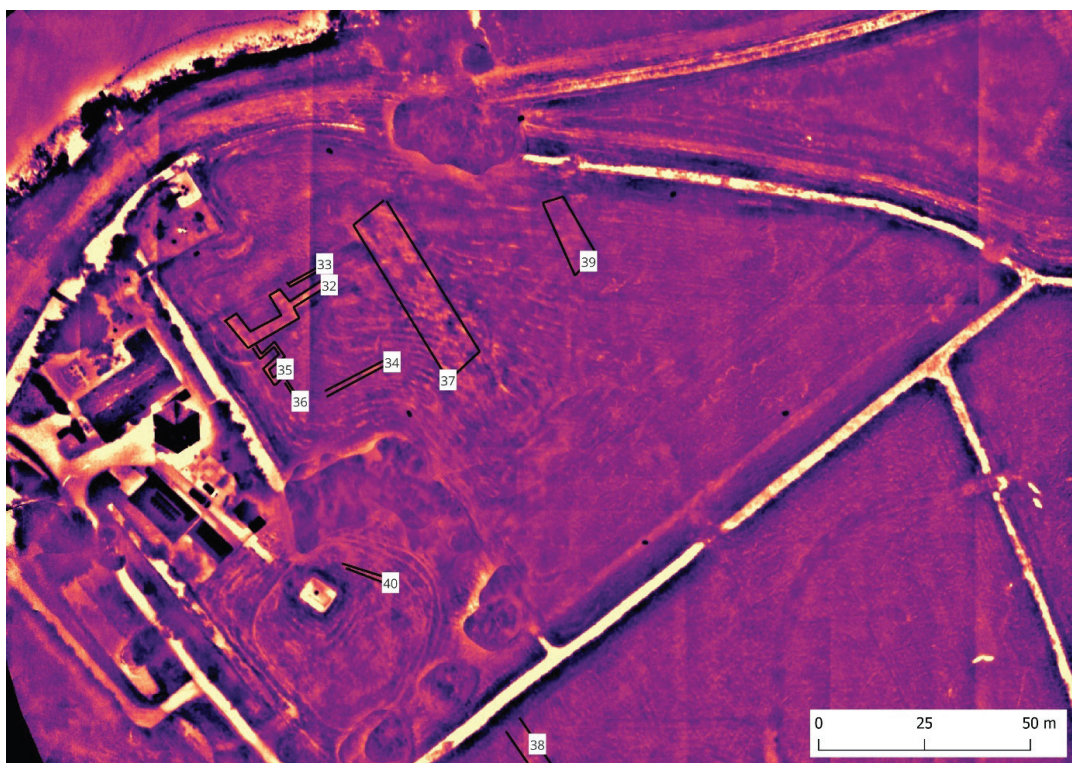
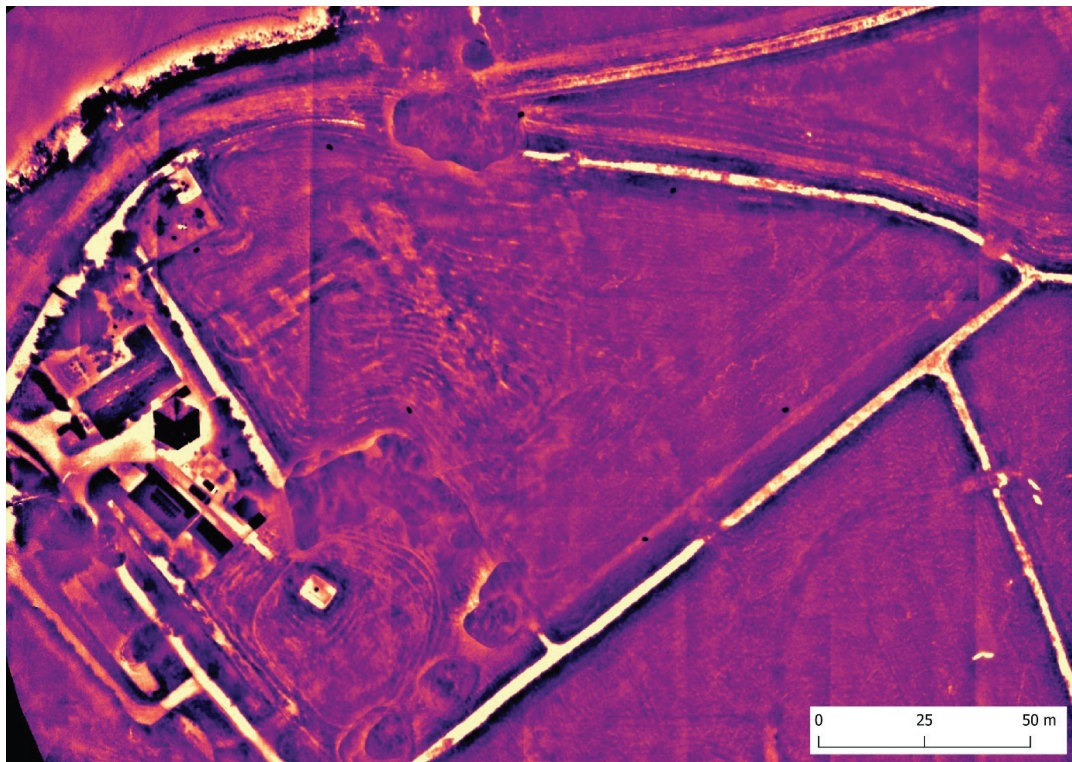
Remarks

Cropmark 9, a brownish vegetation patch (due to drought), is very clearly related to the tower and castle walls. Cropmark 10 is then a bit less neat, patchier, as also in other layers where this anomaly can be observed. It is most likely that it follows the walls of the tower, but possibly the stones here have been removed, resulting in a less clear feature.

Cropmarks 11-13 and 47, also brownish vegetation patches (due to drought), have been marked because they are different from the tractor tracks that are all over the field, in the sense that they are at 1. rectangular in shape and 2. miss a parallel track (that would have been present in case they would be tractor tracks); they are here and there also visible on other layers as well.

Cropmarks 14-15, again visible as stretches of land with more dry vegetation. They match anomalies identified on other layers.

September 2022, thermal mosaic (thermal sensor)



Figures 21-22. Thermal mosaics from September 2022, without and with annotated anomalies.

All mapping (fig. 21-22) by JW, 29-03-2023 (all vegetation densities: 1)

id	source_lay	anoma_int	an_confid	visibility	arch_int	arch_confi
32	therm_120m_ LP_30m	spectral mark, rectangular fea- ture	3	2	stone tower/castle walls	3
33	therm_120m_ LP_30m	spectral mark, rectangular fea- ture	1	2	stone castle struc- tures	1
34	therm_120m_ LP_30m	spectral mark, rectangular fea- ture	2	2	stone castle struc- tures	2
35	therm_120m_ LP_30m	spectral mark, rectangular fea- ture	2	2	stone castle struc- tures	2
36	therm_120m_ LP_30m	spectral mark, rectangular fea- ture	2	2	stone castle struc- tures	2
37	therm_120m_ LP_30m	spectral mark, rectangular patch	3	2	castle wall debris	1
38	therm_120m_ LP_30m	spectral mark, rectangular patch	2	1	ditch	1
39	therm_120m_ LP_30m	spectral mark, rectangular patch	2	1	part of secondary moat	1
40	therm_120m_ LP_30m	spectral mark, rectangular fea- ture	1	2	stone structure	1

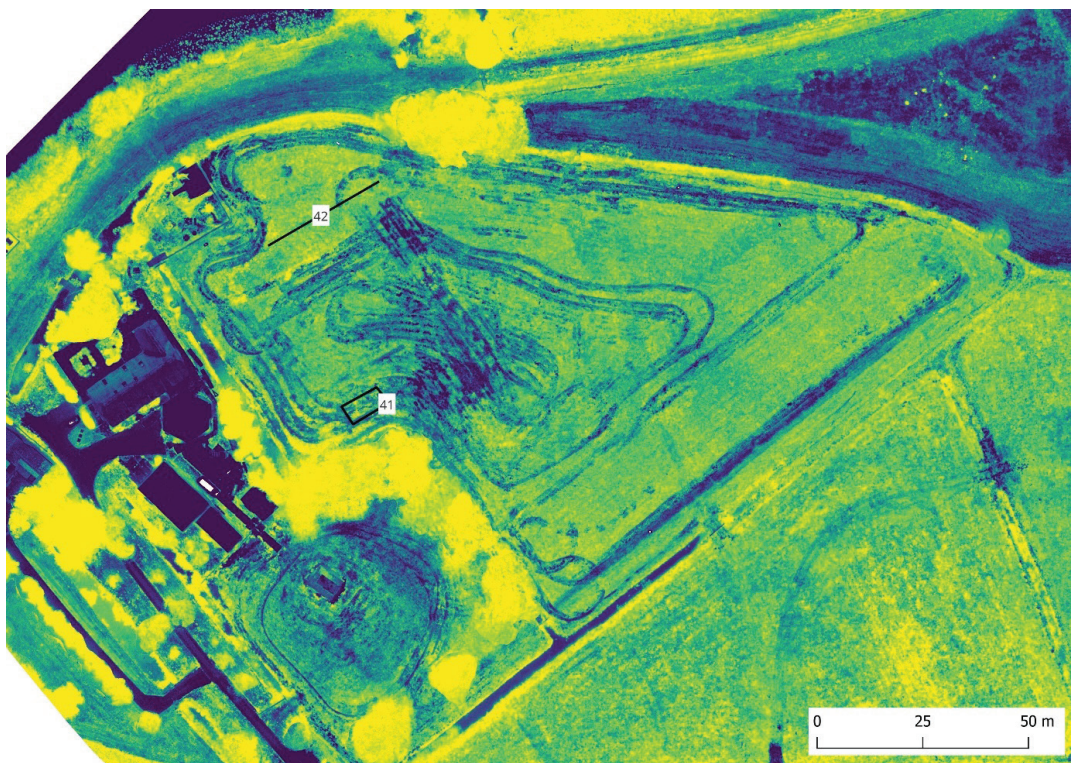
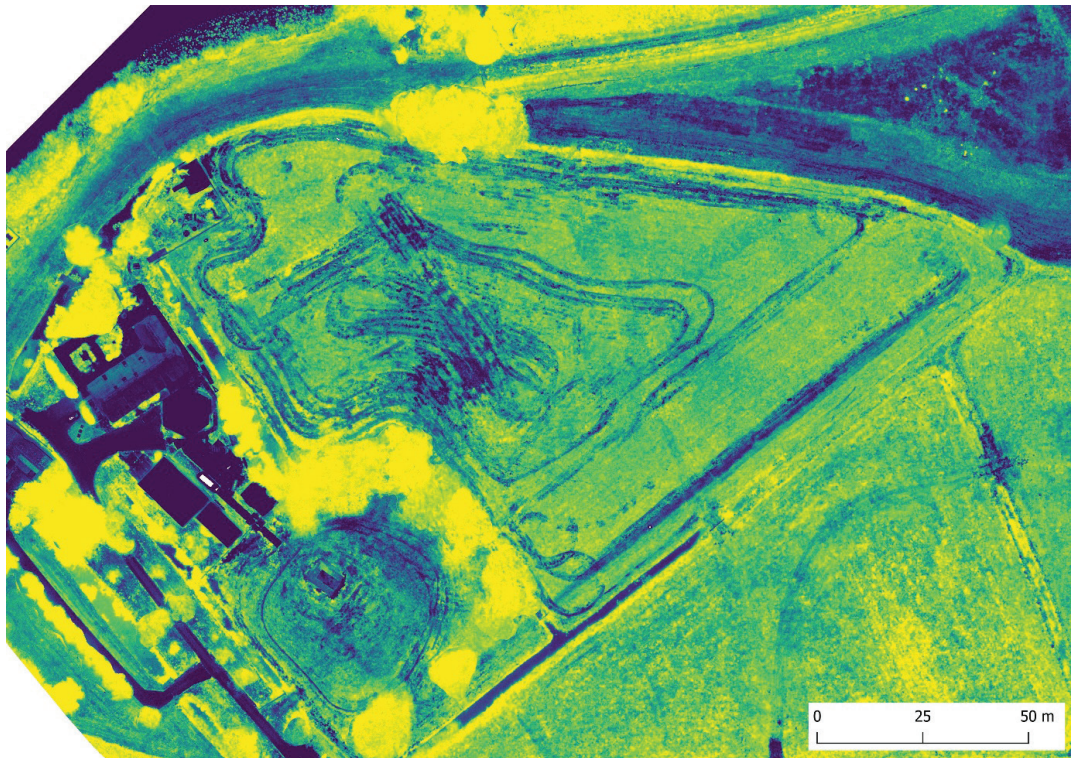
Remarks

All spectral marks identified as anomalies are lighter on the thermal mosaic, meaning that they emit more thermal radiation than the direct surrounding soil matrix. Feature 32 is clearly an anomaly indicating the tower and castle walls, visible because of buried stones that retain a relatively high amount of heat. Anomalies 33-36 are a bit less clear but still due to their shape and orientation appear to signal stone walls. Feature 37 is a broad patch of terrain emitting relatively more thermal radiation that appears to fall inside the moat. This could be either caused by stone building materials, which could corroborate the hypothesis of collapsed debris in the moat, or it could point to a higher moisture retention due to a soil matrix that absorbs more water than the surrounding soil. The latter could point to a later intervention in the soil here.

Anomalies 38 and 39 are elongated broad patches that appear to emit more thermal radiation, where 39 overlaps with the possible ditch identified on the orthophotos and LiDAR visualizations.

Anomaly 40 is quite clear and might point to a subsoil stone feature, but there is no clear archaeological interpretation.

September 2022, NDVI (multispectral sensor)



Figures 23-24. NDVI mosaic from September 2022, without and with annotated anomalies.

All mapping (fig. 23-24) by JW, 29-03-2023 (all vegetation densities: 1)

id	source_lay	anoma_int	an_confid	visibility	arch_int	arch_confid
41	multi_ndvi	cropmark, rectangular dry feature	1	1	stone castle structures	1
42	multi_ndvi	cropmark, linear edge	1	1	edge of moat	0

Remarks

On the NDVI, a few cropmarks have been identified in addition to those already visible on the optical orthophoto but are not visible on any of the other layers. The darker colours indicate vegetation with a lower density/health.

Anomaly 41 appears to have a rectangular shape and is almost parallel to the expected castle walls orientation, therefore it could be a related structure. Anomaly 42 appears to be a vague edge but is so faint that it cannot be reasonably interpreted as something archaeological.

4.1.4 Deep interpretation

Based on the drone remote sensing results, the presence of buried stone structures can be clearly confirmed and extended. On all data layers, optical, multispectral and thermal, the northern, western and southern castle walls have been discerned. It appears that part of the western wall are also several stone structures inside the castle walls.

Also, as for the surrounding terrain, the moat is clearly discernible as a distinct shape in the DEMs, as well as some ditches and less clear but certainly manmade earthworks in the field towards the east. One of these ditches may be interpreted as a possible second moat, and the other features may be related to other infrastructure related to the castle site, although due to their uncertain interpretation and date, may very well be of later origin. Although vague, there appears to be stone material in the primary moat, that on the LiDAR appears to form a rectangular line and may point to a collapsed wall.

Finally, the remote sensing data also appears to indicate post-depositional activity on the site. The various round patches with diverging vegetation are located exactly on top of the supposed trajectory of the castle walls, suggesting an effort to dig (remove stones?) at that location.

In conclusion, the drone remote sensing data corroborates the identification of the castle as an early motte and bailey type, with a clearly defined moat. There may have been more buildings, but their presence is not indicated by the collected data, although there are traces that may point to related Medieval infrastructure.

There has yet been no further physical assessment or any automated recognition operation on the site/data.

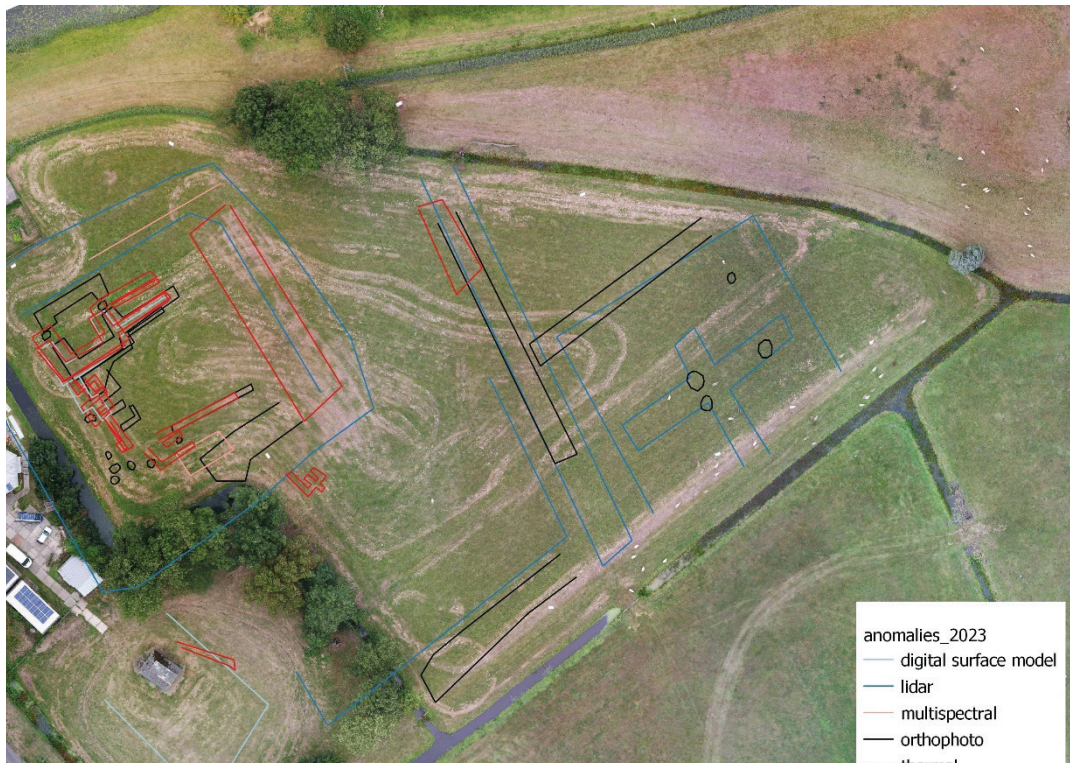


Figure 25. Optical mosaic from September 2022, with all identified anomalies (grouped per data model).

4.1.5 Conclusion

The drone remote sensing operations have produced clear traces of subsoils deposits relating to the castle, varying from clear castle walls to probably stone walls, a very clear delineation of the moat, a possible second moat, postdepositional disturbances and some less easy to interpret rectangular and linear traces.

As for the methodological comparison, some interesting observations can be made. First of all, the grass growth cycle of this cool-season grass, is such that in June it is at the peak of its growth, and both for the optical and multispectral survey, does not really result in any clear expression of cropmarks aside from the already evident traces of the castle tower and abutting walls. Spectral marks however are traceable in the thermal infrared imagery. Although much more diffuse than in the Autumn recordings, clear features that are probably stone (castle) walls can be identified. The most probable reason for this is that due to a relatively high diurnal temperature flux (4-19 degrees C.) shallow stone features do get heated up during the day quicker than the surrounding clayey soil, and due to their higher volumetric heat capacity can store more heat. Therefore, they emit more thermal infrared radiation in the early evening, which is even discernible as spectral marks even if diffused by the relatively high vegetation.

The September flights appear to have produced the most informative data. Due to the maximum stress induced by the draught late summer 2022, cropmarks were very clear, even if partly obscured by the mowing activity. The optical and multispectral data produce very clear cropmarks. Also, the thermal infrared mosaic features

very clear thermal anomalies. Although the diurnal temperature flux was less extreme than in Spring (13-18 degrees C.), the dry soil and dry low (mown) vegetation makes for a superficial layer with a high thermal conductivity, allowing buried materials with a contrasting thermal emission to be well visible. The LiDAR recordings that were made did not give a very remarkably different view of the terrain morphology than the AHN3 data, although features are quite more clearly delineated allowing for more detail to be observed. It must be mentioned though that this was an experimental recording, with some clear calibration flaws, and will improve in the near future.

The February recordings were actually expected to be executed in the least favourable conditions, with a cloudy sky, very wet circumstances and low and little variable temperatures between day and night. However, the rain caused moist conditions that actually created some marks here and there, as patches of water remained on the ground. Also, various cropmarks were visible, which were not clear in September due to the tracks of the tractor. Unfortunately for comparison reasons, the thermal survey could not take place. As for the DSM generated using photogrammetry, this produced actually the clearest earthworks in winter. This is probably the result of the low vegetation, and the fact that the LiDAR data were noisy due to the collection procedure, otherwise one would expect these techniques to result in similar data models.

5 Dissemination and archiving

5.1 *Data management*

All data is stored at the 4D Research Lab archive, cloud storage (MS Teams/Sharepoint), facility of the UvA. In the near future, the original data will be published on the UvA Figshare environment. Original raw material is saved alongside all derived products. These consist of calibrated images (.jpg, .tif), field measurements (.txt), photogrammetry project files and related data (.p4d, .qgz), LiDAR data (.ldr, .las, the latter also tiled), and raster products such as orthophotos, DEMs/DTMs, Vis, etc. (geo-tiff, .tif). The total project size is ca. 315 GB. The 4DRL uses a standardized GIS folder structure, but still has to implement a metadata schema for individual files.

5.2 *Dissemination*

This report will be published open access through the 4D Research Lab Report Series, a Figshare hosted Journal, and be provided with a DOI. As such, existing metadata will be preserved, and the data will be rendered as FAIR as possible.

5.3 *Archiving*

As for archiving, as mentioned, all raw data will eventually be made available via Figshare. In addition, the project data will remain available at the cloud storage facility of the UvA (MS Teams/Sharepoint). All data will be kept available for use/re-use upon any reasonable request.

Bibliography

Hill, A.C., Laugier, E., Casana, J. Archaeological Remote Sensing Using Multi-Temporal, Drone Acquired Thermal and Near Infrared (NIR) Imagery: A Case Study at the Enfield Shaker Village, New Hampshire. *Remote Sens.* 2020, 12, 690.

Jayasena, R.M., 2023 (in prep.). Power games and conspiracies in Amsterdam's 13th-century urban development, *Amsterdam, XII. Lübecker Kolloquium zur Stadtarchäologie im Hanseraum*.

Lozić, E., Štular, B., 2021. Documentation of Archaeology-Specific Workflow for Airborne LiDAR Data Processing. *Geosciences* 11, no. 1: 26. <https://doi.org/10.3390/geosciences11010026>

Rensink, E., Theunissen, L., Feiken, R., Bourgeois, J., Deforce, K., van Doesburg, J., Emaus, R., van der Heiden, M., de Jong-Lambregts, N., Karagiannis, N., de Kort, J.W., Liagre, E., van Londen, H., Meylemans, E., Orbons, J., Stichelbaut, B., Terlouw, B., Timmermans, G., Waagen, J. van Zijverden, W., 2022. *Vanuit de lucht zie je meer. Remote sensing in de Nederlandse archeologie*. Nederlandse Archeologische Rapporten (NAR) 80.

Sapirstein, P., Murray, S., 2017. Establishing best practices for photogrammetric recording during archaeological fieldwork. *J. Field Archaeol.* 42 (4), 337–350. <https://doi.org/10.1080/00934690.2017.1338513>

Waagen, J., García Sánchez, J., van der Heiden, M., Kuiters, A., Lulof, P., 2022. In the Heat of the Night: Comparative Assessment of Drone Thermography at the Archaeological Sites of Acquarossa, Italy, and Siegerswoude, The Netherlands. *Drones* 6, no. 7: 165. <https://doi.org/10.3390/drones6070165>

Appendix 1, data capture parameters

February 2022

Project planning	Title	Huis ten Bosch, Weesp
	Brief description	Castle site examination
	Purpose	Determine state, type and extent of subsoil remains
	Platform	Multirotor
	Date of flight(s)	9-2-2022
	Operator	UvA Dronelab (4DRL)
	Pilot in Command	Jitte Waagen
	Observers	Tijm Lanjouw, Markus Stoffer

Optical survey

System calibration	Sensor type	Optical, CMOS, 4/3"
	Scanner/camera model	Zenmuse X5S
	Lens	15mm
	Shutter type	Rolling (fast readout)
	Instruments	DJI M210, Geomax Zenith15 dGPS
	Pixels	20.8MP
	Precision	5280x3956
	Accuracy	N/A
Data acquisition	Time	12.00
	Exposure triangle	Aperture Priority (f/2.8)
	Altitude Above Ground Level	45m
	Average Speed	3.5m/s
	Overlap (side- and front)	70% and 80%
	Estimated type archaeology	Stone walls, ditches
	Estimated depth archaeology	10-100cm
	Vegetation type	Grassland
	Vegetation state	Dormant
	Moisture conditions	Very wet (rain)
	Superficial layer	Light clay
	Soil matrix	Light clay
	Light conditions	Overcast
	Number of photos	436
	Format	JPG
Geometric correction	Flight trajectory calculation (software/method)	DJI Pilot/grid
	GCPs used	6
	GCP geolocation instrument	Geomax Zenith15, 06GPS

	GCP geolocation accuracy	1-2cm
	GCP and photo merging	Pix4D
	Coordinate system	Amersfoort/RD New (EGM 96 Geo-id), EPSG: 28992
Radiometric correction	N/A	N/A

Multispectral survey

System calibration	Sensor type	Multispectral, 4/3"
	Scanner/camera model	Micasense Rededge
	Centre bandwidths	B (475), G (560), R (668), RE (717), NIR (840)
	Lens	5.4mm
	Shutter type	Global (all sensors)
	Instruments	DJI M210, Geomax Zenith15 dGPS, Downwelling Light Sensor 2
	Pixels	1.2MP (all sensors)
	Precision	1280x960 (all sensors)
	Accuracy	N/A
Data acquisition	Time	11.20
	Exposure triangle	Automated
	Altitude Above Ground Level	45m
	Average Speed	3m/s
	Overlap (side- and front)	70% and 80%
	Estimated type archaeology	Stone walls, ditches
	Estimated depth archaeology	10-100cm
	Vegetation type	Grassland
	Vegetation state	Dormant
	Moisture conditions	Very wet (rain)
	Superficial layer	Light clay
	Soil matrix	Light clay
	Light conditions	Overcast
	Number of photos	4257
	Format	TIF
Geometric correction	Flight trajectory calculation (software/method)	DJI Pilot/grid
	GCPs used	6
	GCP geolocation instrument	Geomax Zenith15, 06GPS
	GCP geolocation accuracy	1-2cm
	GCP and photo merging	Pix4D
	Coordinate system	Amersfoort/RD New (EGM 96 Geo-id), EPSG: 28992
Radiometric correction	Downwelling Light Sensor used	yes

Calibration reflectance panel	yes
Processing and calibration	Pix4D
Setting	Camera, Sun Irradiance and Sun Angle using DLS IMU

Thermal infrared survey

System calibration	Sensor type	Thermal Infrared, Uncooled Vox Microbolometer, 4/3"
	Scanner/camera model	Zenmuse XT2, radiometric (Float32)
	Lens	9mm
	Shutter type	Global
	Instruments	DJI M210, Geomax Zenith15 dGPS
	Pixels	307.2KP
	Precision	640x512
	Accuracy	N/A
Data acquisition	Time	19.00, flight aborted due to bad visibility conditions
	Exposure triangle	Automated
	In-flight calibration	Automatic FFC correction
	Altitude Above Ground Level	45m, 120m
	Average Speed	3.5m/s
	Overlap (side- and front)	75% and 85%
	Estimated type archaeology	Stone walls, ditches
	Estimated depth archaeology	10-100cm
	Vegetation type	Grassland
	Vegetation state	Dormant
	Moisture conditions	Very wet (rain)
	Relative humidity	75%
	Superficial layer	Light clay
	Soil matrix	Light clay
	Light conditions	After sunset
	Temperature current	9
	Temperature max	11
	Temperature min	8
	Number of photos	694
	Format	R_JPG
Geometric correction	Flight trajectory calculation (software/method)	DJI Pilot/grid
	GCPs used	6
	GCP geolocation instrument	Geomax Zenith15, 06GPS
	GCP geolocation accuracy	1-2cm
	GCP and photo merging	Pix4D
Radiometric correction	Processing and calibration	FLIR Thermal Studio Pro

Setting	Distance, temperature, relative humidity setting, and noise removal
---------	---

June 2022

Project planning	Title	Huis ten Bosch, Weesp
	Brief description	Castle site examination
	Purpose	Determine state, type and extent of subsoil remains
	Platform	Multirotor
	Date of flight(s)	2-6-2022
	Operator	UvA Dronelab (4DRL)
	Pilot in Command	Jitte Waagen
	Observers	Mikko Kriek

Multispectral survey

System calibration	Sensor type	Multispectral, 4/3"
	Scanner/camera model	Micasense Rededge
	Centre bandwidths	B (475), G (560), R (668), RE (717), NIR (840)
	Lens	5.4mm
	Shutter type	Global (all sensors)
	Instruments	DJI M210, Geomax Zenith15 dGPS, Downwelling Light Sensor 2
	Pixels	1.2MP (all sensors)
	Precision	1280x960 (all sensors)
	Accuracy	N/A
Data acquisition	Time	13.15
	Exposure triangle	Automated
	Altitude Above Ground Level	50m
	Average Speed	3m/s
	Overlap (side- and front)	70% and 80%
	Estimated type archaeology	Stone walls, ditches
	Estimated depth archaeology	10-100cm
	Vegetation type	Grassland
	Vegetation state	Peak growth
	Moisture conditions	Dry
	Superficial layer	Light clay
	Soil matrix	Light clay
	Light conditions	Clear
	Number of photos	2395
	Format	TIF

Geometric correction	Flight trajectory calculation (software/method)	DJI Pilot/grid
	GCPs used	16
	GCP geolocation instrument	Geomax Zenith15, 06GPS
	GCP geolocation accuracy	1-2cm
	GCP and photo merging	Pix4D
	Coordinate system	Amersfoort/RD New (EGM 96 Geoid), EPSG: 28992
Radiometric correction	Downwelling Light Sensor used	yes
	Calibration reflectance panel	yes
	Processing and calibration	Pix4D
	Setting	Camera, Sun Irradiance and Sun Angle using DLS IMU

Thermal infrared survey

System calibration	Sensor type	Thermal Infrared, Uncooled Vox Microbolometer, 4/3"
	Scanner/camera model	Zenmuse XT2, radiometric (Float32)
	Lens	9mm
	Shutter type	Global
	Instruments	DJI M210, Geomax Zenith15 dGPS
	Pixels	307.2KP
	Precision	640x512
	Accuracy	N/A
Data acquisition	Time	22.00
	Exposure triangle	Automated
	In-flight calibration	Automatic FFC correction
	Altitude Above Ground Level	50m, 100m
	Average Speed	3.5m/s
	Overlap (side- and front)	75% and 85%
	Estimated type archaeology	Stone walls, ditches
	Estimated depth archaeology	10-100cm
	Vegetation type	Grassland
	Vegetation state	Peak growth
	Moisture conditions	Dry
	Relative humidity	72%
	Superficial layer	Light clay
	Soil matrix	Light clay
	Light conditions	After sunset
	Temperature current	13
	Temperature max	19
	Temperature min	4

	Number of photos	1043 (50m), 67 (100m)
	Format	R_JPG
Geometric correction	Flight trajectory calculation (software/method)	DJI Pilot/grid
	GCPs used	16
	GCP geolocation instrument	Geomax Zenith15, 06GPS
	GCP geolocation accuracy	1-2cm
	GCP and photo merging	Pix4D
Radiometric correction	Processing and calibration	FLIR Thermal Studio Pro
	Setting	Distance, temperature, relative humidity setting, and noise removal

September 2022

Project planning	Title	Huis ten Bosch, Weesp
	Brief description	Castle site examination
	Purpose	Determine state, type and extent of subsoil remains
	Platform	Multirotor
	Date of flight(s)	9-9-2022
	Operator	UvA Dronelab (4DRL)
	Pilot in Command	Jitte Waagen
	Observers	Tijm Lanjouw

Optical survey

System calibration	Sensor type	Optical, CMOS, 4/3"
	Scanner/camera model	Zenmuse X5S
	Lens	15mm
	Shutter type	Rolling (fast readout)
	Instruments	DJI M210, Geomax Zenith15 dGPS
	Pixels	20.8MP
	Precision	5280x3956
	Accuracy	N/A
Data acquisition	Time	11.30
	Exposure triangle	Aperture Priority (f/2.8)
	Altitude Above Ground Level	50m
	Average Speed	3.5m/s
	Overlap (side- and front)	70% and 80%
	Estimated type archaeology	Stone walls, ditches
	Estimated depth archaeology	10-100cm
	Vegetation type	Grassland
	Vegetation state	Stressed (drought), mown
	Moisture conditions	Dry
	Superficial layer	Light clay
	Soil matrix	Light clay
	Light conditions	Scattered small clouds
	Number of photos	346
	Format	JPG/RAW
Geometric correction	Flight trajectory calculation (software/method)	DJI Pilot/grid
	GCPs used	6
	GCP geolocation instrument	Geomax Zenith15, 06GPS
	GCP geolocation accuracy	1-2cm
	GCP and photo merging	Pix4D
	Coordinate system	Amersfoort/RD New (EGM 96 Geoid), EPSG: 28992
Radiometric correction	N/A	N/A

Multispectral survey

System calibration	Sensor type	Multispectral, 4/3"
	Scanner/camera model	Micasense Rededge
	Centre bandwidths	B (475), G (560), R (668), RE (717), NIR (840)
	Lens	5.4mm
	Shutter type	Global (all sensors)
	Instruments	DJI M210, Geomax Zenith15 dGPS, Downwelling Light Sensor 2
	Pixels	1.2MP (all sensors)
	Precision	1280x960 (all sensors)
	Accuracy	N/A
Data acquisition	Time	10.30
	Exposure triangle	Automated
	Altitude Above Ground Level	70m
	Average Speed	3m/s
	Overlap (side- and front)	70% and 80%
	Estimated type archaeology	Stone walls, ditches
	Estimated depth archaeology	10-100cm
	Vegetation type	Grassland
	Vegetation state	Stressed (drought), mown
	Moisture conditions	Dry
	Superficial layer	Light clay
	Soil matrix	Light clay
	Light conditions	Scattered small clouds
	Number of photos	1495
	Format	TIF
Geometric correction	Flight trajectory calculation (software/method)	DJI Pilot/grid
	GCPs used	6
	GCP geolocation instrument	Geomax Zenith15, 06GPS
	GCP geolocation accuracy	1-2cm
	GCP and photo merging	
	Coordinate system	Amersfoort/RD New (EGM 96 Geoid), EPSG: 28992
Radiometric correction	Downwelling Light Sensor used	yes
	Calibration reflectance panel	yes
	Processing and calibration	Pix4D
	Setting	Camera, Sun Irradiance and Sun Angle using DLS IMU

Thermal infrared survey

System calibration	Sensor type	Thermal Infrared, Uncooled Vox Microbolometer, 4/3"
	Scanner/camera model	Zenmuse XT2, radiometric (Float32)
	Lens	9mm
	Shutter type	Global
	Instruments	DJI M210, Geomax Zenith15 dGPS
	Pixels	307.2KP
	Precision	640x512
	Accuracy	N/A
Data acquisition	Time	20.00
	Exposure triangle	Automated
	In-flight calibration	Automatic FFC correction
	Altitude Above Ground Level	120m
	Average Speed	3.5m/s
	Overlap (side- and front)	75% and 85%
	Estimated type archaeology	Stone walls, ditches
	Estimated depth archaeology	10-100cm
	Vegetation type	Grassland
	Vegetation state	Stressed (drought), mown
	Moisture conditions	Dry
	Relative humidity	75%
	Superficial layer	Light clay
	Soil matrix	Light clay
	Light conditions	After sunset
	Temperature current	16
	Temperature max	18
	Temperature min	13
	Number of photos	307
	Format	R_JPG
Geometric correction	Flight trajectory calculation (software/method)	DJI Pilot/grid
	GCPs used	6
	GCP geolocation instrument	Geomax Zenith15, 06GPS
	GCP geolocation accuracy	1-2cm
	GCP and photo merging	Pix4D
Radiometric correction	Processing and calibration	FLIR Thermal Studio Pro
	Setting	Distance, temperature, relative humidity setting, and noise removal

LiDAR survey

System calibration	Sensor type	Discrete-return LiDAR
	Scanner/camera model	Zenmuse L1, Livox LiDAR module
	Instruments	DJI M300, D-RTK 2 Mobile Station
	Pulse repetition rate	240 kHz in 2 return mode, 160 kHz in 3 return mode
	Wavelength	905nm
	Point rate	Multiple return: max. 480.000pts
	Additional sensors	Optical camera (20 MP, 4864x3648 (4/3"), 8.8mm, Global shutter)
	Accuracy (max. scanning angle error)	Horizontal: 10cm @ 50m; Vertical: 5cm @50 m
	INS angle accuracy	Yaw Accuracy (RMS 1): Real-time: 0.3°, Post-processing: 0.15° Pitch/Roll Accuracy (RMS 1): Real-time: 0.05°, Post-processing: 0.025°
	INS-GNSS-laser synchronisation error	N/A
Data acquisition	Time	12.30
	Altitude Above Ground Level	50m
	Average Speed	5m/s
	Swath width	30m
	Flight strip overlap	20%
	Footprint diameter	N/A
	Average laser pulse density per m2	1200
	N/E/H accuracy (precision) (m)	N/A
	Number of flight strips	9
	Estimated type archaeology	Stone walls, ditches
	Estimated depth archaeology	10-100cm
	Vegetation type	Grassland
	Vegetation state	Stressed (drought), mown
	Moisture conditions	Dry
	Superficial layer	Light clay
	Soil matrix	Light clay
	Light conditions	Scattered small clouds
	Number of points	Ca. 122.000.000
	Format	.txt
Geometric correction	Flight trajectory calculation (software/method)	DJI Pilot/grid/DGPS
	GCPs used	N/A
	GNSS geolocation instrument	D-RTK 2 Mobile Station

	GNSS geolocation accuracy	1-2cm
	Raw data analysis	DJI Terra
	Merging of raw data with flight trajectory	DJI Terra
	GNSS and IMU merging	DJI Terra
	Full-Waveform Processing and Filtering	N/A
	LAS export	DJI Terra
	LAS format	1.4
	Coordinate system	Amersfoort/RD New (EGM 96 Geoid), EPSG: 28992
Radiometric correction	Processing and calibration	N/A
	Setting	N/A

Appendix 2, data processing parameters

February 2022

Optical survey

PG: Import/reference	Software	Pix4D Mapper 4.5.7
	Batch/Chunks	1
	Geolocated images	492
	Quality check	Manual
	CRS camera	WGS84 (EGM 96 Geoid), EPSG: 4326
	CRS GCPs	Amersfoort/RD New (EGM 96 Geoid), EPSG: 28992
	CRS output	Amersfoort/RD New (EGM 96 Geoid), EPSG: 28992
	Camera model	FC6520_DJIMFT115mmF1.7AS-PH_15.0_5280x3956
	Geolocation accuracy	Horz: 5m Vert: 10m
	Manual corrections	Set altitude to 45m
	Mean Reprojection Error	0.204 pixels
	GCPs used	6
	GCP accuracy	mean RMS error = 0.009m
PG: Alignment/sparse PC	Keypoint Image Scale	Full
	Calibrated/aligned images	492
	Matching type	Aerial Grid or Corridor
	Matching settings	None
	Key point extraction	Automatic (10.000 per image)
	Tie point extraction	N/A
	Calibration method	Standard
	Int. parameters optim.	All
	Ext. parameters optim.	All
	Rematch	Auto
PG: Dense PC	Other settings	N/A
	Image scale/quality	Multiscale, ½ (half image size, default)
	Point density	Optimal
	Minimum # of matches	3
	Number of points	57.901.670
	Classification	Yes (Pix4D method)
PG: 3D model	Other settings	N/A
	Source data	PC
	Surface type	N/A
	Octree depth	High (14)
	Face count	High (max. 5.000.000)
	Texture size	High (16384x16384)
	Texture source data	N/A

	Texture type	N/A
	Mapping mode	N/A
	Blending mode	N/A
	Colour balancing	No
	Other settings	N/A
PG: ortho	GSD	1.02cm/pixel
	Source data	N/A
	Blending mode	N/A
	Other settings	N/A
PG: DSM	GSD	1.02cm/pixel
	Source data	N/A
	Noise filter	Yes
	Surface smoothing	Yes
	Type	Sharp
	Method	IDW
PG: DTM	GSD	1.02cm/pixel
	Point classes	N/A
PG: index	GSD	N/A
	Radiom. correction type	N/A
	Calibration	N/A
	Reflectance map	N/A
	Index and calculation	N/A
Enhanced visualisation	Software	QGIS 3.28.0
	Visualisation	Multiband colour
	Colour ramp	N/A
	Processing	None
	Filter	None
	Settings	None

Multispectral survey

PG: Import/reference	Software	Pix4D Mapper 4.5.7
	Batch/Chunks	5 (R/G/B/RE/NIR)
	Geolocated images	4255
	Quality check	Manual
	CRS camera	WGS84 (EGM 96 Geoid), EPSG: 4326
	CRS GCPs	Amersfoort/RD New (EGM 96 Geoid), EPSG: 28992
	CRS output	Amersfoort/RD New (EGM 96 Geoid), EPSG: 28992
	Camera model	RedEdge-M_5.5_1_1280x960 (R/G/B/RE/NIR)
	Geolocation accuracy	Horz: 5m Vert: 10m
	Manual corrections	Set altitude to 45m
	Mean Reprojection Error	0.249 pixels

	GCPs used	6
	GCP accuracy	mean RMS error = 0.021m
PG: Alignment/sparse PC	Keypoint Image Scale	Full
	Calibrated/aligned images	4220
	Matching type	Aerial Grid or Corridor
	Matching settings	None
	Key point extraction	Automatic (10.000 per image)
	Tie point extraction	N/A
	Calibration method	Alternative
	Int. parameters optim.	All
	Ext. parameters optim.	All
	Rematch	Auto
	Other settings	N/A
PG: Dense PC	Image scale/quality	Multiscale, ½ (half image size, default)
	Point density	Low
	Minimum # of matches	3
	Number of points	1.446.143
	Classification	No
	Other settings	N/A
PG: 3D model	Source data	N/A
	Surface type	N/A
	Octree depth	N/A
	Face count	N/A
	Texture size	N/A
	Texture source data	N/A
	Texture type	N/A
	Mapping mode	N/A
	Blending mode	N/A
	Colour balancing	N/A
	Other settings	N/A
PG: ortho	GSD	N/A
	Source data	N/A
	Blending mode	N/A
	Other settings	N/A
PG: DSM	GSD	N/A
	Source data	N/A
	Noise filter	N/A
	Surface smoothing	N/A
	Type	N/A
	Method	N/A
PG: DTM	GSD	N/A
	Point classes	N/A
PG: index	GSD	3.4cm/pixel

	Radiom. correction type	Camera and Sun Irradiance using DLS IMU
	Calibration	Yes (with reflectance target)
	Reflectance map	Yes
	Index and calculation	R, G, B, RE, NIR $NDVI = (NIR-R)/(NIR+R)$
Enhanced vis.: DSM	Software	QGIS 3.28.0
	Visualisation	Singleband pseudocolour
	Colour ramp	Td/DEM_poster (8 colours)
	Processing	None
	Filter	DSM – local cumulative cut stretch (set by window extents, default settings)
	Settings	None

Thermal infrared survey

No data processing due to aborted flight

June 2022

Multispectral survey

PG: Import/reference	Software	Pix4D Mapper 4.5.7
	Batch/Chunks	5 (R/G/B/RE/NIR)
	Geolocated images	2390
	Quality check	Manual
	CRS camera	WGS84 (EGM 96 Geoid), EPSG: 4326
	CRS GCPs	Amersfoort/RD New (EGM 96 Geoid), EPSG: 28992
	CRS output	Amersfoort/RD New (EGM 96 Geoid), EPSG: 28992
	Camera model	RedEdge-M_5.5_1_1280x960 (R/G/B/RE/NIR)
	Geolocation accuracy	Horz: 5m Vert: 10m
	Manual corrections	Set altitude to 50m
	Mean Reprojection Error	0.190 pixels
	GCPs used	16
	GCP accuracy	mean RMS error = 0.038m
PG: Alignment/sparse PC	Keypoint Image Scale	Full

	Calibrated/aligned images	2350
	Matching type	Aerial Grid or Corridor
	Matching settings	None
	Key point extraction	Automatic (10.000 per image)
	Tie point extraction	N/A
	Calibration method	Alternative
	Int. parameters optim.	All
	Ext. parameters optim.	All
	Rematch	Auto
	Other settings	N/A
PG: Dense PC	Image scale/quality	Multiscale, ½ (half image size, default)
	Point density	Low
	Minimum # of matches	3
	Number of points	894.576
	Classification	No
	Other settings	N/A
PG: 3D model	Source data	N/A
	Surface type	N/A
	Octree depth	N/A
	Face count	N/A
	Texture size	N/A
	Texture source data	N/A
	Texture type	N/A
	Mapping mode	N/A
	Blending mode	N/A
	Colour balancing	N/A
	Other settings	N/A
PG: ortho	GSD	N/A
	Source data	N/A
	Blending mode	N/A
	Other settings	N/A
PG: DSM	GSD	N/A
	Source data	N/A
	Noise filter	N/A
	Surface smoothing	N/A
	Type	N/A
	Method	N/A
PG: DTM	GSD	N/A
	Point classes	N/A
PG: index	GSD	3.46cm/pixel
	Radiom. correction type	Camera and Sun Irradiance using DLS IMU
	Calibration	Yes (with reflectance target)
	Reflectance map	Yes

	Index and calculation	R, G, B, RE, NIR NDVI = (NIR-R)/(NIR+R)
Enhanced visualisation	Software	No
	Visualisation	None
	Colour ramp	None
	Processing	None
	Filter	None
	Settings	None

Thermal infrared survey

PG: Import/reference	Software	Pix4D Mapper 4.5.7
	Batch/Chunks	1
	Geolocated images	67
	Quality check	Manual
	CRS camera	WGS84 (EGM 96 Geoid), EPSG: 4326
	CRS GCPs	Amersfoort/RD New (EGM 96 Geoid), EPSG: 28992
	CRS output	Amersfoort/RD New (EGM 96 Geoid), EPSG: 28992
	Camera model	XT2_13.0_640x512 (Grayscale)
	Geolocation accuracy	Horz: 5m Vert: 10m
	Manual corrections	Set altitude to 100m
	Mean Reprojection Error	0.710 pixels
	GCPs used	9
	GCP accuracy	mean RMS error = 3.638m
PG: Alignment/sparse PC	Keypoint Image Scale	Full
	Calibrated/aligned images	67
	Matching type	Aerial Grid or Corridor
	Matching settings	None
	Key point extraction	Automatic (10.000 per image)
	Tie point extraction	N/A
	Calibration method	Alternative
	Int. parameters optim.	All
	Ext. parameters optim.	All
	Rematch	Auto
PG: Dense PC	Other settings	N/A
	Image scale/quality	Multiscale, 1 (original image size, slow)
	Point density	Optimal
	Minimum # of matches	3
	Number of points	346.445
	Classification	No
	Other settings	N/A

PG: 3D model	Source data	N/A
	Surface type	N/A
	Octree depth	N/A
	Face count	N/A
	Texture size	N/A
	Texture source data	N/A
	Texture type	N/A
	Mapping mode	N/A
	Blending mode	N/A
	Colour balancing	N/A
	Other settings	N/A
PG: ortho	GSD	N/A
	Source data	N/A
	Blending mode	N/A
PG: DSM	Other settings	N/A
	GSD	N/A
	Source data	N/A
PG: DTM	Noise filter	N/A
	Surface smoothing	N/A
	Type	N/A
	Method	N/A
	GSD	N/A
PG: index	Point classes	N/A
	GSD	22.88cm/pixel
	Radiom. correction type	No Correction
	Calibration	N/A
	Reflectance map	Yes
Enhanced visualisation	Index and calculation	N/A
	Software	QGIS 3.28.0
	Visualisation	Singleband pseudocolour
	Colour ramp	Magma
	Processing	Calculated a low pass 30m filter, subtracted the filter from the layer to reduce the global temperature flux and enhance local contrast
	Filter	Local cumulative cut stretch (set by window extents, default settings)
	Settings	None

September 2022

Optical survey

PG: Import/reference	Software	Pix4D Mapper 4.5.7
	Batch/Chunks	1
	Geolocated images	346
	Quality check	Manual
	CRS camera	WGS84 (EGM 96 Geoid), EPSG: 4326
	CRS GCPs	Amersfoort/RD New (EGM 96 Geoid), EPSG: 28992
	CRS output	Amersfoort/RD New (EGM 96 Geoid), EPSG: 28992
	Camera model	FC6520_DJIMFT115mmF1.7AS-PH_15.0_5280x3956
	Geolocation accuracy	Horz: 5m Vert: 10m
	Manual corrections	Set altitude to 50m
	Mean Reprojection Error	0.234 pixels
	GCPs used	6
	GCP accuracy	mean RMS error = 0.011m
PG: Alignment/sparse PC	Keypoint Image Scale	Full
	Calibrated/aligned images	346
	Matching type	Aerial Grid or Corridor
	Matching settings	None
	Key point extraction	Automatic (10.000 per image)
	Tie point extraction	N/A
	Calibration method	Standard
	Int. parameters optim.	All
	Ext. parameters optim.	All
	Rematch	Auto
	Other settings	N/A
PG: Dense PC	Image scale/quality	Multiscale, ½ (half image size, default)
	Point density	Optimal
	Minimum # of matches	3
	Number of points	37.530.548
	Classification	Yes (Pix4D method)

	Other settings	N/A
PG: 3D model	Source data	PC
	Surface type	N/A
	Octree depth	High (14)
	Face count	High (max. 5.000.000)
	Texture size	High (16384x16384)
	Texture source data	N/A
	Texture type	N/A
	Mapping mode	N/A
	Blending mode	N/A
	Colour balancing	No
	Other settings	N/A
PG: ortho	GSD	1.60cm/pixel
	Source data	N/A
	Blending mode	N/A
	Other settings	N/A
PG: DSM	GSD	1.60cm/pixel
	Source data	N/A
	Noise filter	Yes
	Surface smoothing	Yes
	Type	Sharp
	Method	IDW
PG: DTM	GSD	1.60cm/pixel
	Point classes	N/A
PG: index	GSD	N/A
	Radiom. correction type	N/A
	Calibration	N/A
	Reflectance map	N/A
	Index and calculation	N/A
Enhanced visualisation	Software	QGIS 3.28.0
	Visualisation	Multiband colour
	Colour ramp	N/A
	Processing	None
	Filter	None
	Settings	None

Multispectral survey

PG: Import/reference	Software	Pix4D Mapper 4.5.7
	Batch/Chunks	5 (R/G/B/RE/NIR)
	Geolocated images	1495
	Quality check	Manual
	CRS camera	WGS84 (EGM 96 Geoid), EPSG: 4326
	CRS GCPs	Amersfoort/RD New (EGM 96 Geoid), EPSG: 28992
	CRS output	Amersfoort/RD New (EGM 96 Geoid), EPSG: 28992
	Camera model	RedEdge-M_5.5_1_1280x960 (R/G/B/RE/NIR)
	Geolocation accuracy	Horz: 5m Vert: 10m
	Manual corrections	Set altitude to 70m
	Mean Reprojection Error	0.234 pixels
	GCPs used	6
	GCP accuracy	mean RMS error = 0.035m
PG: Alignment/sparse PC	Keypoint Image Scale	Full
	Calibrated/aligned images	2350
	Matching type	Aerial Grid or Corridor
	Matching settings	None
	Key point extraction	Automatic (10.000 per image)
	Tie point extraction	N/A
	Calibration method	Alternative
	Int. parameters optim.	All
	Ext. parameters optim.	All
	Rematch	Auto
	Other settings	N/A
PG: Dense PC	Image scale/quality	Multiscale, ½ (half image size, default)
	Point density	Low
	Minimum # of matches	3
	Number of points	490.788
	Classification	No
	Other settings	N/A
PG: 3D model	Source data	N/A
	Surface type	N/A
	Octree depth	N/A
	Face count	N/A
	Texture size	N/A
	Texture source data	N/A
	Texture type	N/A
	Mapping mode	N/A
	Blending mode	N/A
	Colour balancing	N/A

	Other settings	N/A
PG: ortho	GSD	N/A
	Source data	N/A
	Blending mode	N/A
	Other settings	N/A
PG: DSM	GSD	N/A
	Source data	N/A
	Noise filter	N/A
	Surface smoothing	N/A
	Type	N/A
	Method	N/A
PG: DTM	GSD	N/A
	Point classes	N/A
PG: index	GSD	7.21cm/pixel
	Radiom. correction type	Camera and Sun Irradiance using DLS IMU
	Calibration	Yes (with reflectance target)
	Reflectance map	Yes
	Index and calculation	R, G, B, RE, NIR $NDVI = (NIR - R) / (NIR + R)$
Enhanced visualisation	Software	QGIS 3.28.0
	Visualisation	Singleband pseudocolour
	Colour ramp	Viridis
	Processing	None
	Filter	Local cumulative cut stretch (set by window extents, default settings)
	Settings	None

Thermal infrared survey

PG: Import/reference	Software	Pix4D Mapper 4.5.7
	Batch/Chunks	1
	Geolocated images	301
	Quality check	Manual
	CRS camera	WGS84 (EGM 96 Geoid), EPSG: 4326
	CRS GCPs	Amersfoort/RD New (EGM 96 Geoid), EPSG: 28992
	CRS output	Amersfoort/RD New (EGM 96 Geoid), EPSG: 28992
	Camera model	XT2_13.0_640x512 (Grayscale)
	Geolocation accuracy	Horz: 5m Vert: 10m
	Manual corrections	Set altitude to 120m
	Mean Reprojection Error	0.761 pixels
	GCPs used	6

	GCP accuracy	mean RMS error = 0.301m
PG: Alignment/sparse PC	Keypoint Image Scale	Full
	Calibrated/aligned images	67
	Matching type	Aerial Grid or Corridor
	Matching settings	None
	Key point extraction	Automatic (10.000 per image)
	Tie point extraction	N/A
	Calibration method	Alternative
	Int. parameters optim.	All
	Ext. parameters optim.	All
	Rematch	Auto
	Other settings	N/A
PG: Dense PC	Image scale/quality	Multiscale, 1 (original image size, slow)
	Point density	Optimal
	Minimum # of matches	3
	Number of points	346.445
	Classification	No
	Other settings	N/A
PG: 3D model	Source data	N/A
	Surface type	N/A
	Octree depth	N/A
	Face count	N/A
	Texture size	N/A
	Texture source data	N/A
	Texture type	N/A
	Mapping mode	N/A
	Blending mode	N/A
	Colour balancing	N/A
	Other settings	N/A
PG: ortho	GSD	N/A
	Source data	N/A
	Blending mode	N/A
	Other settings	N/A
PG: DSM	GSD	N/A
	Source data	N/A
	Noise filter	N/A
	Surface smoothing	N/A
	Type	N/A
	Method	N/A
PG: DTM	GSD	N/A
	Point classes	N/A
PG: index	GSD	16.64cm/pixel
	Radiom. correction type	No Correction
	Calibration	N/A

	Reflectance map	Yes
	Index and calculation	N/A
Enhanced visualisation	Software	QGIS 3.28.0
	Visualisation	Singleband pseudocolour
	Colour ramp	Magma
	Processing	Calculated a low pass 30m filter, subtracted the filter from the layer to reduce the global temperature flux and enhance local contrast
	Filter	Local cumulative cut stretch (set by window extents, default settings)
	Settings	None

LiDAR survey

Conversion	Software	LAStools Rapidlasso GmbH
	Tool	Tiling
	Filter	None
	Settings	20m
	Script	lastile -i *.las -tile_size 20 -buffer 2 -odir 1-tiles -o tile.laz
Automatic ground point classification	Software	LAStools Rapidlasso GmbH
	Tool	Ground point
	Filter	Ground point
	Settings	Extra fine, Wilderness
	Script	lasground -i *.laz -odir 2-ground -o ground.laz -extra_fine -wilderness
DTM	Software	LAStools Rapidlasso GmbH
	Tool	DEM
	Filter	None
	Settings	Resolution 0.005m, ignore triangles of >50m
	Script	las2dem -i *.laz -odir 3-dem -o dem.tif -use_tile_bb -keep_class 2 -step 0.005 -kill 50
Merge	Software	QGIS 3.28.0
	Tool	Merge
	Filter	None
	Settings	None
	Script	None
Enhanced visualisation	Software	QGIS 3.28.0
	Visualisation	Singleband pseudocolour
	Colour ramp	NRWC
	Processing	None

Filter	Local cumulative cut stretch (set by window extents, default settings)
Settings	None

Appendix 3, schema of documented metadata for anomaly mapping and interpretation

Item	Description	Values	Comments
Id	Anomaly number	1-x	Simple enumerator
Rec_moment	Recording moment	E.g., 'winter', 'February, or a more specific date	Used to organize GIS layers
Sensor_vi	Sensor Visualisation	E.g., 'opt_ortho' (optical sensor, orthophoto visualization) or 'multi_ndvi' (multispectral sensor, NDVI visualization)	The sensor and the specific data model used for the mapping of anomalies; refers to 4.1.2 Data processing and derivation of products
Source_lay	Source Layer	E.g., 'dem_1cmres' (LiDAR DEM data with a 1cm resolution) or 'autumn_120m_corrected_with_LP_30m' (Thermal mosaic recorded at 120m with a Low Pass filter using a 30m radius)	The specific visualization of the data used for the mapping of anomalies; refers back to 4.1.2 Data processing and derivation of products
Anoma_int	Interpretation of anomaly source	E.g., 'ditch outline', 'rectangular elevation', 'subsoil stone feature'	Initial mapping of all features that are not explained by not directly explained by natural or modern anthropomorphic activity
An_confid	Confidence of anomaly interpretation	0-3	'0' none (anomaly type is unknown), '1' low (anomaly interpretation is questionable), '2' medium (anomaly is clearly visible and there are analogies to the confirmed interpretation in the area, but the morphology is not distinct), '3' high (anomaly clearly visible and has a distinct form (adapted from Lozić and Štular 2021))
Visibility	How well is the anomaly visible	1-2	Referring to the local contrast that led to identification of the anomaly; '1' is poor and '2' is good (adapted from Lozić and Štular 2021)
Veget_dens	How dense is the vegetation locally	1-3	Referring to local vegetation density that may obscure full identification of the anomaly; '1' negligible, '2' medium (introduces occasional and/or moderate noise) or '3' high (introduces constant and/or significant noise) (adapted from Lozić and Štular 2021)
Author	Author	E.g., 'JW' (Jitte Waagen)	The person that performs the anomaly and interpretative mapping

Date	Date	E.g., '12-04-2023'	Date of the anomaly and interpretative mapping
Arch_int	Archaeological interpretation of anomaly	E.g., 'moat outline', 'structure boundary', 'stone debris of collapsed wall'	Interpretation of anomaly in terms of the most probable archaeological explanation
Arch_confi	Confidence of archaeology interpretation	0-3	<p>'0' none (interpretation is very uncertain), '1' low (interpretation is questionable), '2' medium (interpretation is plausible and there are analogies to the confirmed</p> <p>interpretation in the area, but the morphology is not distinct), '3' high (interpretation is quite certain and has a distinct form (adapted from Lozić and Štular 2021)</p>

